The Cryosphere, 20, 6613–6634, 2026
https://doi.org/10.5194/tc-20-6613-2026
© Author(s) 2026. This work is distributed under
the Creative Commons Attribution 4.0 License.

The Cryosphere Open Access EGU

Improved CMIP6 projections of Hudson Bay region navigability using bias correction and route continuity

Armina Soleymani[1], **Alex Crawford**[1], **Lawrence Mudryk**[2], **and Feiyue Wang**[1]

[1]Department of Environment and Geography, Centre for Earth Observation Science, Riddell Faculty of Earth, Environment and Resources, University of Manitoba, Winnipeg, Canada
[2]Climate Research Division, Environment and Climate Change Canada, Toronto, Canada

Correspondence: Armina Soleymani (armina.soleymani@umanitoba.ca)

Received: 14 July 2026 – Discussion started: 23 July 2026
Revised: 4 November 2026 – Accepted: 6 November 2026 – Published: 16 November 2026

Abstract. Hudson Bay's seasonal sea ice limits maritime access to the Port of Churchill. This study improves on past efforts to project future navigability of shipping routes from Churchill by correcting for substantial model biases, better combining sea ice concentration (SIC) and sea ice thickness (SIT) into calculations, and incorporating a novel pathfinding approach that requires continuous navigable routes (rather than relying on spatial domain averages). We evaluate future navigability for type E vessels under two criteria: ice-free and low-risk (applying the Polar Operational Limit Assessment Risk Indexing System, POLARIS). Additionally, we examine both the global shipping route (Churchill-Labrador Sea) and regional connectivity within northwestern Hudson Bay (Churchill-Chesterfield Inlet). In the 1980s, median navigable periods (NPs) for the Churchill-Labrador route were 102 d (ice-free) and 123 d (low-risk), compared to 106 and 123 d, respectively, for the Churchill-Chesterfield route. By 2020–2025, these periods increased by approximately 4 weeks. Various methods of employing POLARIS and climate models yield a range of baseline NPs but consistent trends. Each additional 0.5 °C of global warming extends NPs by 11–19 d up to 3.5 °C, beyond which the rate of increase accelerates. Under 4.5–5.0 °C warming (late 21st century in SSP5-8.5), the Churchill-Labrador Sea route would remain ice-free for up to 265 d (8.8 months), representing an increases of 137 d relative to present conditions. Under low-risk conditions, navigability would reach 304 d (10.1 months), an increase of 147 d. The two bias correction methods produce generally consistent long-term increases but can differ by several weeks in individual projections, highlighting sensitivity to methodological choices. Findings demonstrate that the navigable season extends for all vessel types and year-round shipping would require ice-strengthened vessels throughout the 21st century even with a high-end warming scenario.

1 Introduction

Hudson Bay, characterized by its seasonal sea ice cover, has emerged as a region of significant strategic interest due to its unique combination of geographic, cultural, and socioeconomic attributes, particularly in relation to marine shipping. Central to this is the Port of Churchill, Manitoba, situated on the western shore of Hudson Bay. As the only deep-water Arctic port in North America directly connected to the continental railway network, Churchill serves a vital logistical role for northern communities while holding potential importance within broader regional and global supply chains. Despite nearly a century of operation, the port has historically underperformed relative to its capacity. One constraint is its short operational season, which historically extends from mid-July through October (Andrews et al., 2017), as nearly all historical grain shipments have been via non-ice-strengthened bulk carriers (Andrews et al., 2016). The restricted shipping window imposes limitations on shipping volume and has discouraged sustained investment in port infrastructure.

The limited duration of the navigable period is shaped not only by environmental factors but also by marine insurance frameworks, which rely on historical sea ice climatologies. Between the 1980s and 2010s, the duration of the ice-free season increased by approximately one month, both from

earlier spring breakups and later autumn freeze-ups (Tivy et al., 2011; Crawford et al., 2021). Record-early ice retreat occurred in eastern Hudson Bay in spring 2024 (Soriot et al., 2025). Climate projections suggest that this trend will continue as Arctic warming progresses (Crawford et al., 2021; IPCC, 2021). These shifts are impacting marine ecosystems (Ferguson et al., 2017; Stroeve et al., 2024), while also disrupting the traditional practices of Indigenous communities that depend on sea ice (Laidler and Gough, 2003). At the same time, the lengthening of the open-water season presents new economic opportunities by allowing extended shipping operations within Hudson Bay via the Port of Churchill (Andrews et al., 2017; Babb et al., 2021) and elsewhere (Cook et al., 2026). If these trends continue, they may enhance Hudson Bay's strategic importance in northern shipping and global trade by improving marine access through the Port of Churchill out via Hudson Strait to international markets (Andrews et al., 2016; Lasserre, 2022).

The seasonal cycle of sea ice retreat in summer and advance in autumn, referred to as sea ice phenology, plays a critical role in determining navigational accessibility in polar regions. Both sea ice concentration (SIC) and sea ice thickness (SIT) are key variables that influence the risk to maritime vessels (Mudryk et al., 2021). In Hudson Bay, SIC varies substantially over the year, reaching near-complete coverage in winter, with maximum monthly average SIT typically reaching 1.6 m in April (Crawford et al., 2023). Long-term records of SIC and SIT are derived from multiple sources, including satellite remote sensing, Canadian Ice Service (CIS) charts, and reanalysis products. Passive microwave satellite observations, in particular, have been widely employed to produce SIC datasets, providing continuous, spatially comprehensive coverage essential for detecting long-term trends in sea ice (e.g., Meier et al., 2014; Soleymani and Scott, 2023). Reanalysis products are generated by assimilating observational data into a consistent dynamical model framework over extended periods, offering temporally homogeneous datasets that are less sensitive to changes in observational systems and well suited for historical reconstructions of sea ice conditions (Cocetta et al., 2024).

Climate models participating in the Coupled Model Intercomparison Project Phase 6 (CMIP6; Eyring et al., 2016) provide projections of future SIC and SIT under a range of Shared Socio-economic Pathways (SSPs), allowing assessments of multiple plausible climate futures (O'Neill et al., 2016). Despite their central role in projecting future sea ice conditions, climate models have inherent limitations. Systematic biases in climate model outputs arise from coarse spatial resolution (often > 100 km) and imperfect physical parameterizations (Notz and SIMIP Community, 2020; Roach and Meier, 2024), while internal climate variability adds further uncertainty to sea ice projections (Maslowski et al., 2012; Swart et al., 2015). To address these challenges, ongoing research focuses on developing and applying bias correction techniques aimed at improving the agreement between model simulations and historical observations, thereby enhancing the reliability of future sea ice projections (e.g., Melia et al., 2015; Knutti et al., 2017; Zhao et al., 2020).

Given the strategic importance of Hudson Bay's navigability for regional connectivity, economic development, and integration into global trade networks, coupled with the complex and highly variable nature of sea ice dynamics, there is a clear need for detailed, route-specific navigability assessments. These assessments must integrate both high-quality historical observations and robust future climate projections to inform operational planning and long-term policy decisions. While previous research has highlighted navigability within the Northern Sea Route (e.g., Shibata et al., 2013; Smith and Stephenson, 2013; Wei et al., 2020) and Northwest Passage (e.g., Pizzolato et al., 2016; Cook et al., 2024), the operational implications for the Port of Churchill to critical destinations such as the Labrador Sea and northern coastal communities (e.g., Arviat, Whale Cove, Rankin Inlet, and Chesterfield Inlet) have received little attention.

The only existing assessment of future navigability in Hudson Bay is that of Mudryk et al. (2021); however, several aspects of the methodology warrant further consideration. First, they used a single-model ensemble (CESM1), and a multi-model ensemble from CMIP6 may provide a better sense of future uncertainty (Notz and SIMIP Community, 2020). Second, model bias is not explicitly addressed. As shown by Crawford et al. (2023), neglecting biases in CMIP6 projections would lead to substantial overestimation of the ice-free period in Hudson Bay in the majority of models, in some cases exceeding one month. Correcting these biases is therefore essential to ensure reliable projections of future accessibility. Third, Mudryk et al. (2021) treat navigation routes as broad spatial areas without accounting for the requirement that navigable grid cells form a continuous pathway. This implicitly assumes that if individual grid cells are on average navigable, then a route is navigable. In reality, navigability is inherently a connectivity problem rather than a spatial average condition. Even if the vast majority of grid cells along the shipping route are navigable, this does not guarantee the presence of a viable transit route, as discontinuities like choke points may obstruct passage (Copland et al., 2021; Cook et al., 2024). Neglecting spatial connectivity can therefore lead to overestimation of practical accessibility and fails to capture key operational constraints. Finally, there are multiple ways to treat the open-water fraction of partially ice-covered grid cells (Mudryk et al., 2021; Cook et al., 2024).

Accurate estimation of the navigable period is essential for ensuring safe operations, efficient logistics, reliable economic planning, and realistic climate adaptation in Arctic shipping, as even modest errors can lead to increased operational risks, suboptimal routing decisions, and misinformed infrastructure investments. In light of the above-mentioned limitations, this study aims to improve projections of future maritime accessibility in Hudson Bay by (i) applying bias

correction to CMIP6 model simulations, (ii) implementing a path-finding approach that explicitly requires continuous, traversable routes rather than isolated grid-cell conditions, and (iii) testing the sensitivity of different ways of implementing the Polar Operational Limit Assessment Risk Indexing System (POLARIS). Particular emphasis is placed on key shipping corridors originating from the Port of Churchill, thereby providing a more realistic and decision-relevant assessment of evolving Arctic maritime accessibility.

2 Methods

2.1 Study Area

The study area focuses primarily on maritime routes connecting the Port of Churchill to the Labrador Sea and Chesterfield Inlet (Igluligaarjuk). Three additional northern communities – Arviat, Whale Cove (Tikirarjuaq), and Rankin Inlet (Kangiqliniq) – are considered as supplementary study areas to provide broader regional context. The analysis spans 1979–2099, allowing for an assessment of historical and projected changes in sea ice conditions and how these changes may affect the length and variability of the operational shipping season.

2.2 Datasets

2.2.1 OSISAF SIC

The Ocean and Sea Ice Satellite Application Facility (OSISAF) algorithm (Lavergne et al., 2019) estimates SIC from brightness temperature measurements obtained by passive microwave sensors. The OSISAF SIC data record is widely recognized for its quality and improvements over earlier datasets, establishing it as a widely used benchmark in climate research and as a trusted climate data record product (Lavergne and Down, 2023). In this study, we used the daily OSISAF SIC product (OSI-450-a1 for 1978–2020 and OSI-430-a for 2021–onwards) at a 25 km gridded resolution, available for the period 1979–2025 from the European Organization for the Exploitation of Meteorological Satellites (EUMETSAT, 2025).

2.2.2 PIOMAS SIC & SIT

The Pan-Arctic Ice-Ocean Modeling and Assimilation System (PIOMAS) is a coupled ice-ocean reanalysis (Zhang and Rothrock, 2003). It combines a physical sea ice and ocean model – incorporating ice thickness distribution and dynamics – with data assimilation of observed variables, including sea surface temperature and sea ice concentration, to produce temporally and spatially complete estimates of Arctic sea ice conditions, including SIC and SIT (Soriot et al., 2024). In this study, we employ daily PIOMAS SIC and SIT data spanning from 1979–2025, at a roughly 25 km horizontal resolution from the University of Washington (Polar Science Center, University of Washington, 2025). It is noted that the actual SIT is obtained by dividing the effective (grid cell-averaged) ice thickness by SIC, thereby confining the ice volume to the ice-covered fraction of the grid cell rather than distributing it across the full grid cell area. CIS ice charts are preferred for operational applications because they provide ice-type information directly relevant to navigation. However, the daily digital CIS charts are available only from 2006 onward. Regional CIS charts extend back to approximately 1970, but they are issued at a coarser temporal resolution than the daily timescale on which changes are reported here. Although the magnitude of change could be expressed in weeks, the daily resolution of PIOMAS allows changes to be reported in days. PIOMAS is therefore used for its daily, continuous temporal coverage over the study period rather than as an operationally superior alternative to CIS charts. Because POLARIS requires ice type or thickness information but not specifically chart-derived inputs, PIOMAS-derived ice characteristics can be substituted. The CIS-derived NP can be used as a complementary independent benchmark for evaluating the thickness-based bias correction approach.

2.2.3 CMIP6 SIC & SIT & GSAT

In this study, we used CMIP6 daily SIC, daily SIT, and monthly global surface air temperature (GSAT) data from 16 models that include historical simulations (1850–2014), as well as Shared Socioeconomic Pathways (SSPs) of future climate (2015–2100) (Table S1 in the Supplement) obtained from the Earth System Grid Federation data nodes (The Earth System Grid Federation, 2025). These models provided the three required variables across all four SSPs – SSP1-2.6, SSP2-4.5, SSP3-7.0, and SSP5-8.5 – where the final number denotes the approximate radiative forcing experienced by 2100. Because the complete open-water period cannot be determined without several months of data from the following year, it is not possible to compute this metric for the final year of the historical experiments (2014) or the SSPs (2100). Note that SIT is the actual floe thickness (which is different from CMIP5).

It should be noted that, to preserve the native spatial characteristics of each model and avoid potential artifacts introduced by interpolation, all data were evaluated at their original model resolutions. Consequently, differences among the models may partly reflect variations in spatial resolution and in their representation of complex features, such as narrow channels and coastal areas.

2.3 Shipping Zone Definition

In this study, shipping routes were represented as a 200 km-wide zone (Fig. 1). This buffer was selected to represent regional-scale shipping accessibility rather than a single prescribed track, allowing for spatial variability in potential nav-

igable pathways while providing a consistent framework for comparison across models with different spatial resolutions and grid structures.

Each route is defined by a start and end node, with the start node corresponding to the marine grid cell containing the Port of Churchill and the end node corresponding to the marine grid cell containing the destination point. We examined two distinct shipping corridors: the Churchill-Labrador Sea route, representing international access to global markets, and the Churchill-Chesterfield Inlet route, representing regional connectivity to northern communities, including Arviat, Whale Cove, and Rankin Inlet. For the Churchill-Labrador Sea route, the southern passage through Hudson Strait is currently favored because of its shorter transit distance (Pizzolato et al., 2016). The shipping routes were manually defined in QGIS using ship traffic contour lines for individual vessels, derived from vessel tracking platforms (e.g., MarineTraffic, 2025). These routes were further validated and refined through personal communication with the Arctic Gateway Group (the limited partnership that owns and operates the Port of Churchill) in 2024.

2.4 Navigability Assignment

Two definitions are used to define navigability: First, with the "ice-free definition", a grid cell within the shipping zone is classified as navigable if its SIC is below 15 %. Second, with the "low-risk definition", a combination of SIC and SIT determine whether a grid cell is navigable based on POLARIS, which assigns risk values (RVs) to various ice types (represented by SIT ranges) according to their potential hazard for a given vessel type (IMO Maritime Safety Committee, 2016). RVs range from $+3$ (lowest risk) to -8 (highest risk), enabling operators to assess operational safety across a range of ice conditions (Fig. 2). As SIT increases, the corresponding RVs decrease, indicating higher operational risk in thicker ice regimes. Next, we use the following formula to evaluate the Risk Index Outcome (RIO) in partially ice-covered grid cells

$$\mathrm{RIO} = \mathrm{SIC} \times \mathrm{RV}_{\mathrm{H,S}} + [3 \times (1 - \mathrm{SIC})], \quad (1)$$

where SIC is the sea ice concentration (ranging from 0 or ice-free to 1 or fully ice-covered), $\mathrm{RV}_{\mathrm{H,S}}$ is the risk value corresponding to a specific SIT category H and ship class S as defined in Fig. 2, and the constant 3 represents the risk value assigned to open water for all vessel types. The second term in the equation accounts for the ice-free fraction of the grid cell, which carries minimal navigational risk. A grid cell is considered navigable when $\mathrm{RIO} \geq 0$, indicating acceptable operational risk. Unlike with definitions of ice-free periods based solely on SIC thresholds, with this definition a grid cell is considered low risk (or "navigable") for open-water vessels if $\mathrm{SIC} > 15\,\%$ but SIT is thin enough (e.g., Fig. 2b, Panel B). Grid cells with $\mathrm{SIT} = 0$ or missing values (NaNs) are assigned an RV of 3, consistent with POLARIS guidelines for open water. This ensures that zero thickness is interpreted as ice-free, and that missing SIT data – when corroborated by low SIC – does not artificially increase risk estimates, thereby maintaining operational realism in the assessment. For the ice-free definition, we used OSISAF SIC, whereas for the low-risk definition, we relied on PIOMAS SIC and SIT as the "observational" dataset. Figure 3 illustrates the procedure for transforming RIOs into a mask that delineates regions of low-risk navigation for a type E vessel. To assess the impact of the second term in the RIO equation, we also assess the following

$$\mathrm{RIO} = \mathrm{SIC} \times \mathrm{RV}_{\mathrm{H,S}}, \quad (2)$$

this equation implies that the RV is 0 for the open water part of a cell, making it less permissive than Eq. (1), which uses a value of 3 for open water. In other words, Eq. (2) shows the impact of considering only SIT in determining a grid cell's RIO instead of both SIT and SIC.

Type E vessels (non-ice-strengthened or minimally ice-strengthened vessels) are the primary focus of this study because they historically have been the dominant commercial vessel class operating at the Port of Churchill (Andrews et al., 2016). Standard non-ice-strengthened vessels generally have lower construction, operating, and insurance costs than ice-strengthened vessels, making them more economically attractive for seasonal shipping (Solakivi et al., 2018). Accordingly, the use of type E vessels defines a conservative minimum length for the economically accessible shipping period; longer navigable periods would be achievable by ice-strengthened vessels (see Sect. 3.5).

2.5 Path Continuity Framework

The spatial connectivity framework is built upon a graph-based representation of the route buffer (200 km-wide zone), where each grid cell constitutes a node and adjacent cells are connected through weighted edges (orthogonal or diagonal). Navigability is first determined at the cell level using either the ice-free or low-risk definition, resulting in a binary mask (e.g., Fig. 3; panel e). This mask is then combined with the predefined route buffer to construct a constrained graph in which only admissible cells are retained. To evaluate continuity, a modified A* path-finding algorithm is applied (in Python using the tcod library) to determine whether a continuous path exists between the start and end nodes. A daily route is considered navigable only when a continuous sequence of connected, navigable grid cells form an unbroken path between the origin and destination. In the absence of such connectivity (e.g., sea ice present at a choke point), the route is classified as non-navigable, even if individual cells satisfy the SIC/SIT navigability criteria. This binary classification of daily route availability ($1 =$ continuous path exists; $0 =$ no path), evaluated throughout the year, forms the basis for determining the opening day (OD), closing day (CD), and NP.

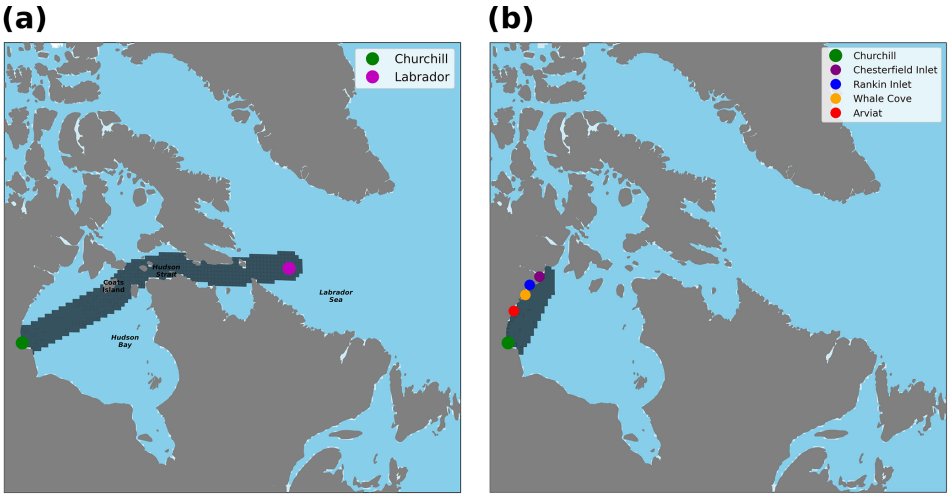


Figure 1. An illustration of the maritime shipping zones allowed for in the study from the Port of Churchill to **(a)** the Labrador Sea, and **(b)** Arviat, Whale Cove, Rankin Inlet, Chesterfield Inlet, with a 200 km-wide zone in dark blue colour (100 km on either side of the route) on the 25 km Equal-Area Scalable Earth grid.

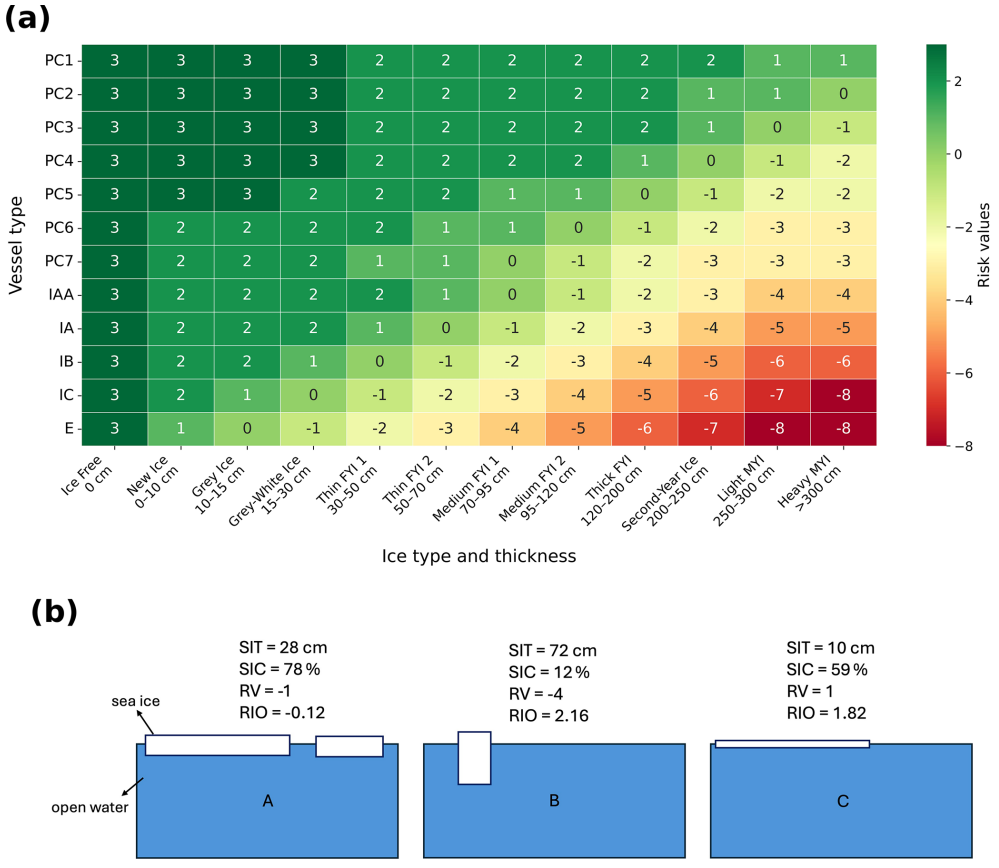


Figure 2. **(a)** Risk values (RVs) for different ice types and vessel types derived from the Polar Operational Limit Assessment Risk Indexing System (POLARIS). **(b)** Navigability assessment for a type E vessel based on sea ice concentration (SIC) and sea ice thickness (SIT) under the "ice-free" and "low-risk" definitions. Panel (A) is not navigable under either definition. Under the ice-free definition, panel (B) is navigable but panel (C) is not. Under the low-risk definition, both panels (B) and (C) are navigable.

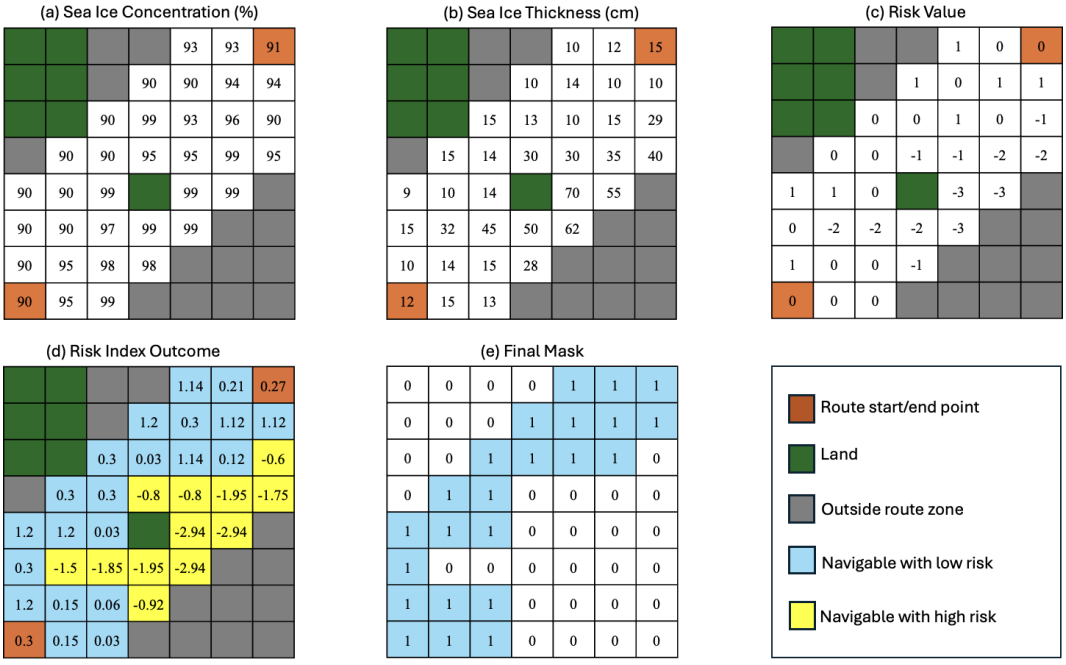


Figure 3. Workflow for deriving type E low-risk navigation mask: **(a)** sea ice concentration (%), **(b)** sea ice thickness (cm), **(c)** risk value, **(d)** risk index outcome, and **(e)** final mask.

2.6 Sea Ice Phenology

For each route and year y, to classify each day as open (navigable) or closed (not navigable) we searched for the main navigable season from 1 January of year y to 30 April of year $y+1$. We defined the median closed day in January to April of year y (mxd1) and year $y+1$ (mxd2), and the median open day in August to November of year y (mnd). The OD is one day after the last closed day between mxd1 and mnd, so short spring openings are skipped. The CD is the first closed day after mnd, up to mxd2. The navigable period or NP is the number of days between them (NP = CD − OD). Routes with no closed day in January to April of both years were classified as open year-round (NP = d yr^{-1}; OD and CD = NaN), and routes with no open day in August to November as closed year-round (NP = 0; OD and CD = NaN). If no closed day was found before mnd, the route starts the year open (OD = NaN; NP = CD − 61), and if none was found after mnd it stays open (CD = NaN; NP = 365+61−OD), truncating NP at about 1 March of years y and $y+1$. The constants 61 and $365+61$ correspond to about 1 March of years y and $y+1$. Figure 4 shows the schematic definition of the OD, CD and NP for a route in year y, together with the special cases

2.7 Model Evaluation

Model performance and internal variability were evaluated for 1979–2013, which corresponds to the overlap between CMIP6 historical runs and the availability of reliable observational datasets (OSISAF and PIOMAS). The multi-model mean of the temporal average (μ_{MMM}) is computed as the average of the first realization ("r1") across all models (except CESM2, for which "r4" is the lowest realization available for all experiments). To estimate internal variability, we leverage the variability from the six single-model ensembles with at least three historical realizations. Because of the small ensemble sizes, we apply a multiplicative correction factor involving the Gamma function (Γ) when calculating the standard deviation of each single-model ensemble, given by

$$\sigma = \frac{s}{c_4(n)}, \tag{3}$$

where s is the sample standard deviation (a biased estimator of the true standard deviation), n is the number of samples (in this case, the number of realizations for the model), and $c_4(n)$ is the bias-correction factor, which can be calculated as

$$c_4(n) = \sqrt{\frac{2}{n-1}} \cdot \frac{\Gamma\left(\frac{n}{2}\right)}{\Gamma\left(\frac{n-1}{2}\right)}. \tag{4}$$

The overall uncertainty of the multi-model mean, denoted as σ_{MMM}, is then estimated as the arithmetic mean of the variability from each single-model ensemble ($\sigma_{model,k}$) across the six qualified models. This aggregated measure is then used to estimate internal variability or IV, and the plausible range of model outcomes around the observational reference value (μ_{obs}) and serves as a benchmark for evaluating model skill and consistency

$$IV = \mu_{obs} \pm 2\sigma_{MMM}. \tag{5}$$

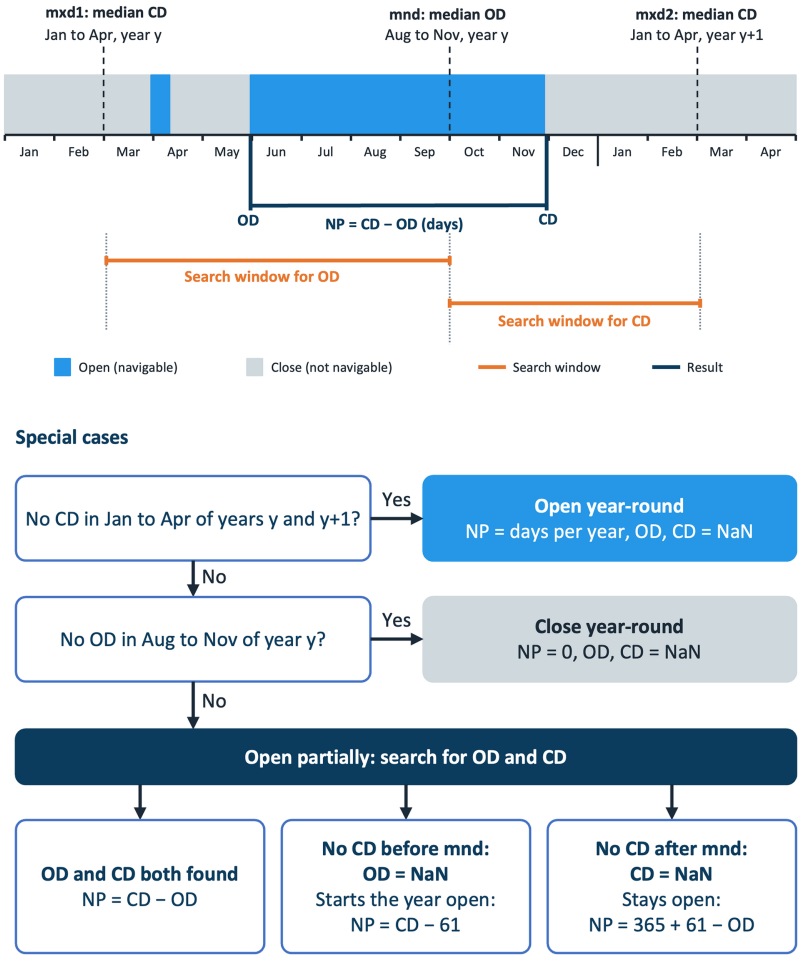


Figure 4. Schematic definition of the opening day (OD), closing day (CD) and navigable period (NP) for a route in year y and the special cases where OD or CD cannot be determined.

Because climate models systematically underestimate sea ice cover in Hudson Bay (Crawford et al., 2023), we applied two common bias correction methods before analyzing projections of future navigability: delta-shift and weighted average.

2.7.1 Bias Correction: Delta-Shift

Delta-shift bias correction adjusts each model by the difference between its historical mean and observations over 1979–2013, aligning the baseline while preserving projected trends. The corrected value is $X_{\mathrm{t}}^{\mathrm{corrected}} = X_{\mathrm{t}} - \Delta$, $\Delta = \mu_{\mathrm{model}} - \mu_{\mathrm{obs}}$. For each route and navigability criterion, the 10th, 50th (median), and 90th percentiles are calculated across the model realizations to characterize the spread of estimated OD, CD, and NP. Model performance is evaluated separately by comparing these results with the corresponding observational reference dataset (OSISAF for the ice-free definition and PIOMAS for the low-risk definition). Only the first realization from each model is used to ensure equal model weighting. See Sect. S1 and Figs. S1 and S2 for details on how the missing data are handled.

2.7.2 Bias Correction: Weighted Average

Our weighting method balances three factors to ensure observational fidelity and a representative spread of projections: model performance (skill) – models are evaluated against observations, with larger errors receiving lower weights; realization similarity (redundancy) – structurally similar models or multiple realizations are down-weighted to avoid over-representation; and model diversity (richness) – an "effective number" constraint prevents over-fitting weights by concentrating on too few high-performing realizations.

Weight Assignment

Weights w_i are calculated following Knutti et al. (2017)

$$w_i = \frac{e^{-D_i^2/\sigma_D^2}}{1 + \sum_{j \neq i}^{M} e^{-S_{ij}^2/\sigma_S^2}}, \tag{6}$$

where D_i is the distance from observations (to account for performance), S_{ij} is the distance between models i and j (to

account for similarity), and σ_D, σ_S are scaling parameters controlling the strength of penalties. The numerator of w_i rewards models close to observations, while the denominator penalizes those similar to others. Finally, model diversity is quantified via the "Effective Size" (N_{eff}), computed as the inverse Simpson Index using the chosen σ_D and σ_S.

Weighted Average

After assigning weights to each model, we computed a weighted average for each sea ice variable at every time step t denoted as $X_{\text{t}}^{\text{corrected}}$ or $\overline{X}_{\text{t}}^{\text{w}}$. Specifically, given the weight w_i for each realization i, the weighted mean is

$$X_{\text{t}}^{\text{corrected}} = \overline{X}_{\text{t}}^{\text{w}} = \frac{\sum w_i X_{\text{t}}^i}{\sum w_i}, \tag{7}$$

where X_{t}^i is the sea ice variable (i.e., OD, CD, NP) from realization i at time t. This formulation ensures that models with greater skill exert proportionally more influence on the final estimate while mitigating the chance of over-fitting, thereby improving the robustness of the model projection.

It is noteworthy that the weights are calibrated using the 1979–2024 climatological means of OD and CD and are subsequently held fixed when applied to the time-varying model projections.

Weighted Standard Error

Uncertainty in $X_{\text{t}}^{\text{corrected}}$ was quantified using the weighted standard error $\text{SE}_{\text{t}}^{\text{w}}$, which incorporates model weights w_i so that more reliable models contribute more. It is defined as

$$\text{SE}_{\text{t}}^{\text{w}} = \sqrt{\frac{\sum w_i \left(X_{\text{t}}^i - \overline{X}_{\text{t}}^{\text{w}}\right)^2}{\sum w_i} \cdot \frac{N-1}{N}}, \tag{8}$$

where X_{t}^i is realization i at time t, $\overline{X}_{\text{t}}^{\text{w}}$ is the weighted mean (Eq. 7), and N is the number of realizations (63 in this study). This adjustment for unequal contributions provides a more accurate measure of realization uncertainty. See Sect. S2 and Figs. S3 and S4 for a detailed description of the experimental setup.

3 Results

3.1 Historical Observations

Before examining future projections, it is instructive to consider the historical baseline navigable period and its trend (Fig. 5). For the Churchill-Labrador Sea route, using the ice-free definition, the median OD shifted earlier from day of year (DOY) 212 (31 July) in the 1980s to 197 (16 July) in the 2000s (−15 d), before moving slightly later again to 199 (18 July) in 2020–2025 (+2 d vs. 2000s, still −13 d compared to the 1980s). The median CD occurred on DOY 314 (10 November) in the 1980s, shifted later to 326 (22 November) in the 2000s (+12 d), and then to 330 (26 November) in 2020–2025 (+4 d vs. 2000s, +16 d vs. 1980s). The median navigable period lengthened from 102 d in the 1980s to 129 d in the 2000s, and further to 131 d in 2020–2025 (+2 d vs. 2000s, +29 d vs. 1980s).

Using the low-risk definition, the median OD shifted earlier from DOY 194 (13 July) in the 1980s to 178 (27 June) in the 2000s (−16 d), and then slightly later to 183 (2 July) in 2020–2025 (+5 d vs. 2000s, still −11 d compared to the 1980s). The median CD occurred on DOY 317 (13 November) in the 1980s, moved later to 330 (26 November) in the 2000s (+13 d), and further to 337 (3 December) in 2020–2025 (+7 d vs. 2000s, +20 d vs. 1980s). The median NP expanded from 123 d in the 1980s, to 152 d in the 2000s (+29 d), and to 154 d in 2020–2025 (+2 d vs. 2000s, +31 d vs. 1980s).

For the Churchill-Chesterfield Inlet route, using the ice-free definition, the median OD shifted earlier from DOY 208 (27 July) in the 1980s to 188 (7 July) in the 2000s (−20 d), then moved later to 199 (18 July) in 2020–2025 (+11 d vs. 2000s). The median CD moved later from DOY 314 (10 November) in the 1980s to 320 (16 November) in the 2000s (+6 d), and to 330 (26 November) in 2020–2025 (+10 d). The median NP lengthened from 106 d in the 1980s to 132 d in the 2000s, then to 131 d in 2020–2025 (−1 d vs. 2000s, +25 d vs. 1980s). Overall, OD advanced and CD delayed from the 1980s to the 2000s, expanding the window, followed by a partial reversal in OD but continued delay in CD into the early 2020s. Using the low-risk definition, the median OD shifted earlier from DOY 190 (9 July) in the 1980s to 169 (18 June) in the 2000s (−21 d), before moving later again to 183 (2 July) in 2020–2025 (+14 d vs. 2000s, still −7 d compared to the 1980s). The median CD was 313 (9 November) in the 1980s, delayed to 322 (18 November) in the 2000s (+9 d), and further to 330 (26 November) in 2020–2025 (+8 d vs. 2000s, +17 d vs. 1980s). The median navigable period lengthened from 123 d in the 1980s to 153 d in the 2000s (+30 d), then shortened to 147 d in 2020–2025 (−6 d vs. 2000s, +24 d vs. 1980s). Because routes to the three communities between Churchill and Chesterfield Inlet – Arviat, Whale Cove, and Rankin Inlet – exhibit broadly comparable temporal patterns and navigability ranges (consistent with their close geographical proximity), detailed analyses for these locations are provided in Supplement Fig. S5.

Altogether, two aspects of change become apparent. First, the navigable period from Churchill to destinations within or beyond Hudson Bay increased markedly (2 to 4 weeks) between the 1980s and 2000s and has been relatively stable since. Second, while the closing day is becoming progressively later with time, the opening day exhibits greater variability and has actually occurred later in recent years than in the 2000s. This variability likely reflects shorter-term internal climate variability rather than a long-term trend. As reported for the Northwest Passage in recent years (Cook et

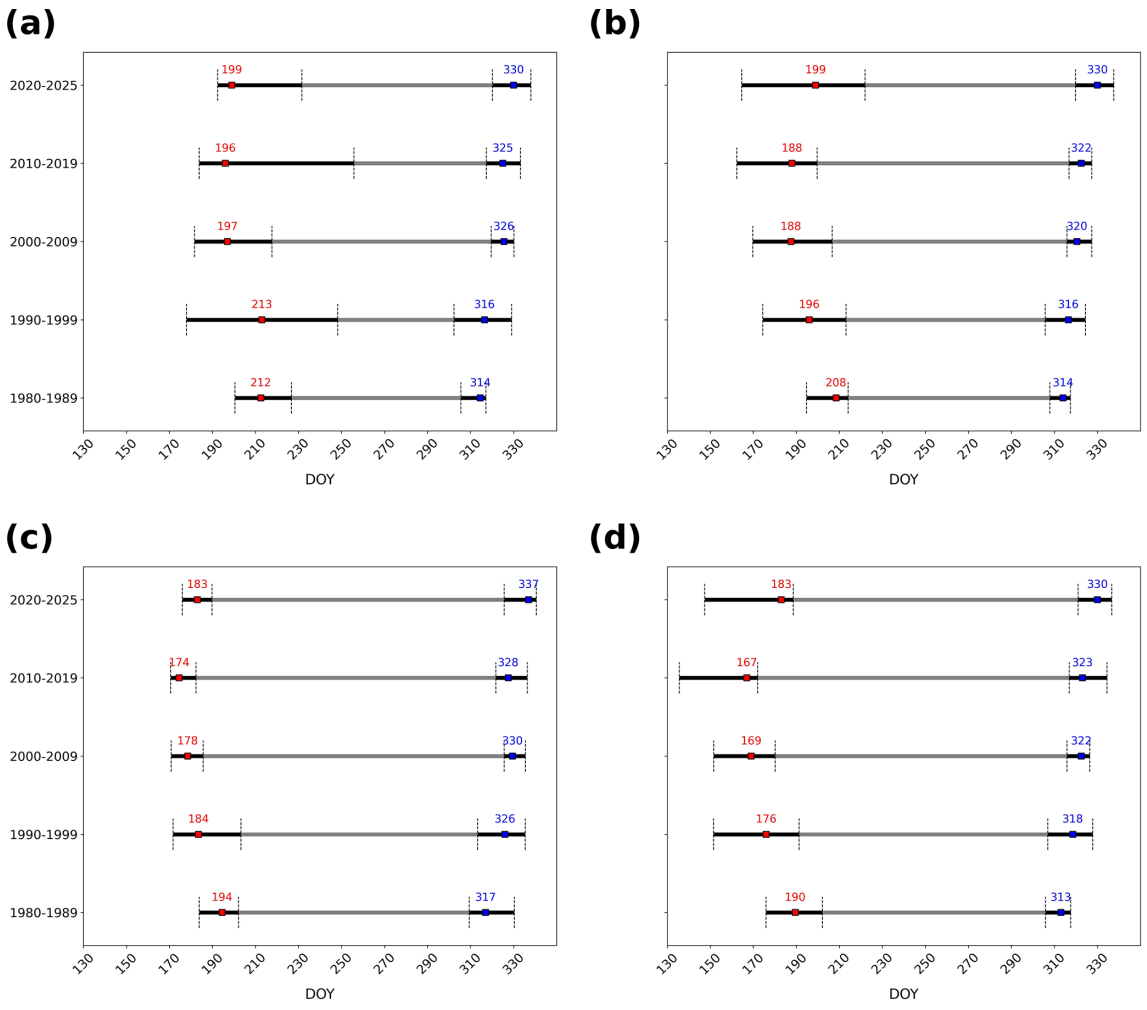


Figure 5. Historical records of opening and closing days (expressed as day of year, DOY) for maritime routes from the Port of Churchill to: **(a)** Labrador Sea (ice-free definition), **(b)** Chesterfield Inlet (ice-free definition), **(c)** Labrador Sea (Type E low-risk definition), and **(d)** Chesterfield Inlet (Type E low-risk definition). Red and blue markers represent the median opening day and closing day, respectively, with the interval between them indicating the median navigation period. Error bars denote the 10th–90th percentile range, and the grey bar highlights the period when the route is reliably navigable, except in extreme years.

al., 2024), dynamic redistribution of sea ice can be highly variable year to year and can block navigability for a route even if only a small section (or "choke point") is blocked. The opening day is more variable than the closing day because it is governed not only by the cumulative impacts of sea ice dynamics, but also by summer sea ice melt processes, both of which are greatly influenced by year-to-year atmospheric variability (Hochheim and Barber, 2014; Crawford et al., 2023).

3.2 Bias Assessment of CMIP6 Models

Figures 6 and 7 present the estimated OD, CD, and NP for the Labrador Sea and Chesterfield Inlet routes, respectively, during the historical period (1979–2013), based on the two definitions. Across both routes, approximately 75 %–87.5 % of the models lie outside the range of internal variability (IV; Eq. 5), shown as whiskers extending from the OSISAF average. This highlights the variability in simulated ice retreat timing and the clear need for bias correction. The ice-free definition generally produces later OD estimates than the low-risk definition, consistent with its stricter single-threshold definition. The Labrador Sea route records the later OD for both the observational mean and multi-model mean, under both definitions. Using the ice-free definition, the models that most closely estimate the observational averages for the Labrador Sea route are ACCESS-CM2, NorESM2-LM, MRI-ESM2-0, and BCC-CSM2-MR, differing by 3–8 d, while for the Chesterfield Inlet route the closest matches are MRI-ESM2-0 and ACCESS-CM2, with deviations of approximately 2–7 d. Under the low-risk definition, the models showing the greatest agreement

with PIOMAS for the Labrador Sea route are IPSL-CM6A-LR, MIROC6, and CESM2, within 1–4 d, whereas for the Chesterfield Inlet route the best matches are ACCESS-CM2 and CESM2- WACCM, within 0.2–3 d.

Similar to OD, most models fall outside the IV range for CD, indicating a significant inter-model spread in the simulated timing of ice advance and highlighting the need for bias correction. CD is overestimated in at least 70 % of realizations. The ice-free definition generally produces earlier CD estimates compared to the low-risk definition. The Labrador Sea route shows the earlier CD for both the observations and multi-model mean under both definitions. For the ice-free definition, the models closest to the observational average for the Labrador Sea route are BCC-CSM2-MR and NorESM2-LM, while for the Chesterfield Inlet route the closest are IPSL-CM6A-LR and NorESM2-LM. Under the low-risk definition, the models nearest to observations for the Labrador Sea route are IPSL-CM6A-LR, NorESM2-LM, and BCC-CSM2-MR, while for the Chesterfield Inlet route they are IPSL-CM6A-LR and NorESM2-MM.

Based on results for OD and CD it is unsurprising that the NP is also biased in most models. NPs are simulated longer than observed in 81 % of models for the Labrador Sea route. For this reason, a delta-shift bias correction (computed as the difference between a model's historical average and the corresponding observational mean) was applied to all projections used in the following section. The low-risk definition generally yields longer NPs than the ice-free definition, consistent with its more permissive navigability definition. For the ice-free definition, the models closest to the observational average for the Labrador Sea route are BCC-CSM2-MR and NorESM2-LM, while for the Chesterfield Inlet route the closest are MRI-ESM2-0, ACCESS-CM2, and NorESM2-MM. Under the low-risk definition, the models nearest to observations for the Labrador Sea route are ACCESS-CM2, IPSL-CM6A-LR, and CESM2-WACCM, within 2–3 d, while for the Chesterfield Inlet route they are the same as the other definition.

Furthermore, when compared with OSISAF, PIOMAS reproduces the overall length of the NP reasonably well, with a maximum difference of nearly 12 d for the Labrador Sea route and a minimum difference of about 2 d for the Chesterfield Inlet route. In contrast, its OD and CD are systematically biased, indicating a misrepresentation of the seasonal timing of sea ice retreat and advance. For OD, the largest difference is seen on the Labrador Sea route, occurring 13 d earlier. For CD, the greatest difference is observed on the Whale Cove route, occurring 10 d earlier. Thus, bias correction based on PIOMAS may be unreliable for OD and CD, but remains appropriate for NP.

The routes to the three communities near Chesterfield Inlet exhibit similar patterns and ranges in OD, CD, and NP, reflecting their geographical proximity. The corresponding results for the Arviat, Whale Cove, and Rankin Inlet routes are presented in Supplement Figs. S6, S7, and S8, respectively.

Turning to long-term change, we also examined trends over the longest period the data allow (1979–2024), following Stroeve et al. (2024). Individual CMIP6 model trends largely fall within the observational uncertainty range, especially for the Churchill to Labrador Sea route. The multi-model mean is a good match to the observed trends except for the generally lower than the observed trend, with the largest gap for Churchill to Chesterfield Inlet route/low-risk definition, where it underestimates the trend. The exceptions are Labrador Sea/ice-free, where it is higher than observed, and Labrador Sea low-risk, where the two are nearly equal (Supplement Fig. S9).

3.3 Navigable Period Projection – Delta-Shift Method

In assessing changes in NP in response to climate change, it is important to recognize that change in NP with respect to time is inherently more uncertain than change in NP with respect to GSAT anomaly. GSAT is a direct function of time under any given forcing pathway, but the rate of change varies substantially among scenarios. As a result, while calendar years associated with specific anomalies differ across SSPs, the anomaly levels themselves are universal. Therefore, we emphasize the relationship between NP and GSAT in this section, although we also show the approximate years at which each GSAT anomaly bin is reached under different SSPs (Table 1). Note that some SSPs do not reach the higher levels of warming within the 21st century.

The projections are derived using delta-shift bias-corrected CMIP6 outputs and evaluated using both navigable route detection criteria: the ice-free definition and the low-risk definition. Each panel in Fig. 8 displays NPs for the corresponding GSAT anomaly bin. The OD_{50} and CD_{50} are shown as red and blue squares, respectively, and the grey bar spanning OD_{90} to CD_{10} denotes the high-confidence NP (i.e., the period for which the route is navigable even in extremely unfavorable simulations).

For the ice-free definition and the 1.0–1.5 °C anomaly bin, representative of the early-century period (2012 to the early 2030s in all SSPs; Table 1), the Labrador Sea route typically opens on DOY 198 (17 July) and closes on DOY 326 (22 November), for a duration of 128 d (about 4.2 months), which is 1–3 d different from OSISAF observations in either 2010–2019 or 2020–2025. Under near-future conditions (1.5–2.0 °C), the Labrador Sea route typically opens on DOY 189 (8 July) and closes on DOY 336 (2 December), yielding an NP of 147 d (approximately 4.9 months), or 19 d longer than present-day. On the extreme end (warming of 4.5–5.0 °C), the Labrador Sea route typically opens on DOY 130 (10 May) and closes on DOY 395 (30 January of the following year), for a duration of 265 d (roughly 8.8 months), about 118 d longer than the near-future and 137 d longer than present-day. Under the low-risk definition, the Labrador Sea route typically opens on DOY 177 (26 June) and closes on DOY 334 (30 November), resulting in 157 d (roughly

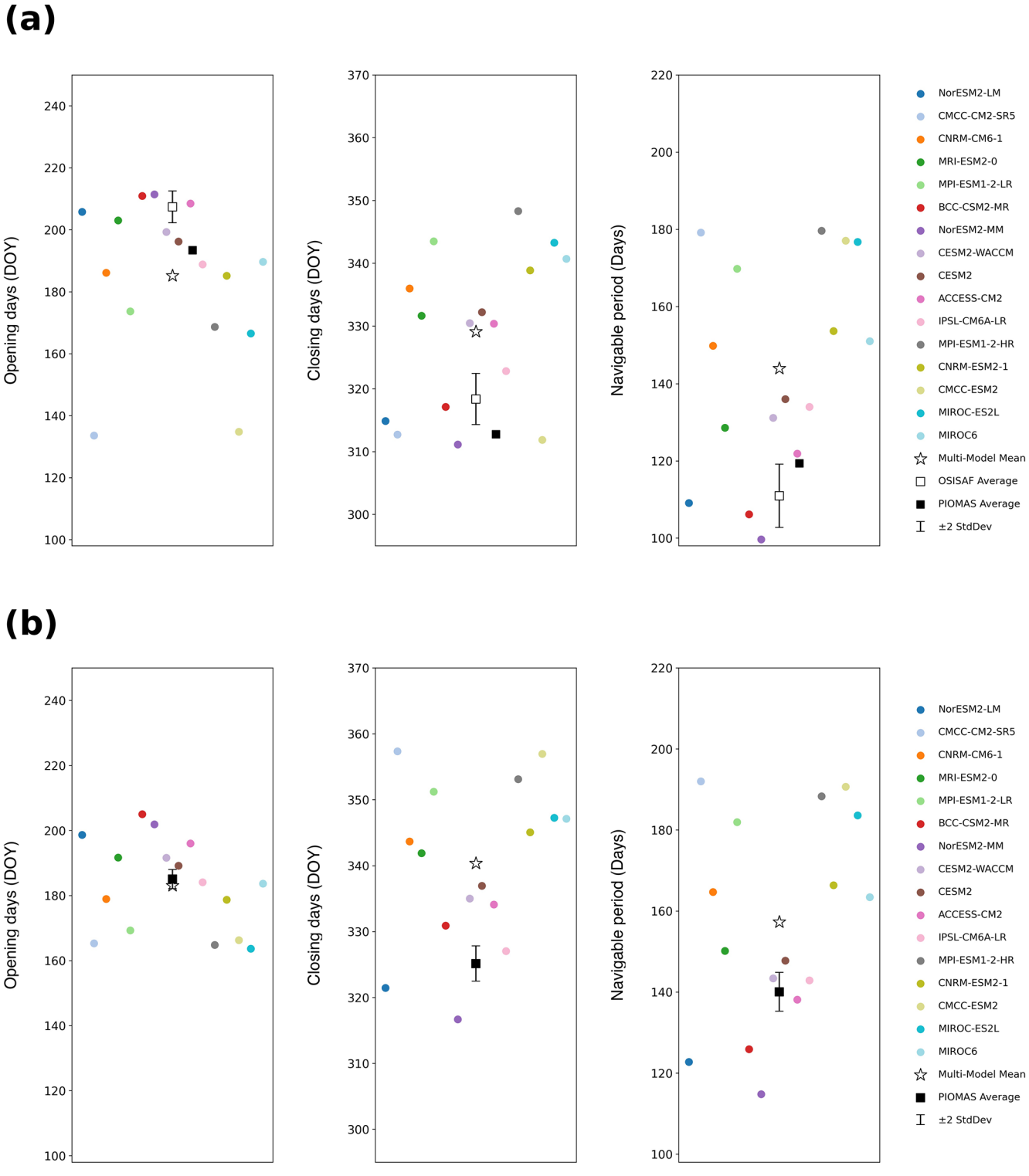


Figure 6. Estimated opening day, closing day, and navigable period for the Churchill-Labrador Sea route, 1979–2013, under **(a)** the ice-free and **(b)** the low-risk definitions.

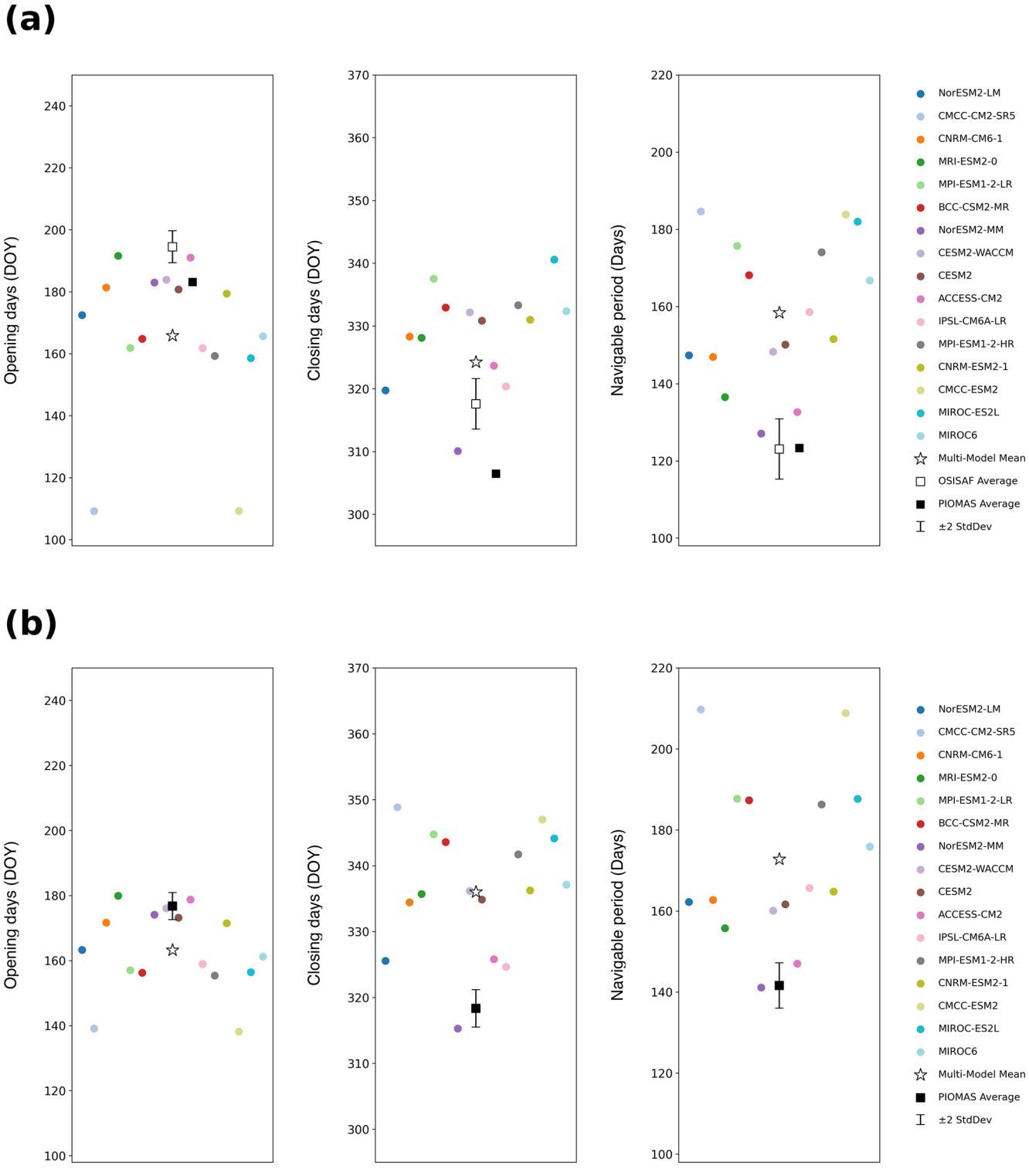


Figure 7. Estimated opening day, closing day, and navigable period for the Churchill-Chesterfield Inlet route, 1979–2013, under **(a)** the ice-free and **(b)** the low-risk definitions.

Table 1. Timing of global surface air temperature (GSAT) anomaly bins (with respect to 1850–1900 average) under each SSP scenario.

Period	GSAT anomaly (°C)	Year			
		SSP1-2.6	SSP2-4.5	SSP3-7.0	SSP5-8.5
Past (historical)	0–1	1950–2011	1950–2011	1950–2011	1950–2011
Present (early-century)	1–1.5	2012–2033	2012–2033	2012–2032	2012–2030
Near-future	1.5–2	2034–2099	2034–2054	2033–2047	2031–2045
	2–2.5	***	2055–2079	2048–2063	2046–2055
	2.5–3	***	2080–2099	2064–2076	2056–2065
	3–3.5	***	***	2077–2088	2066–2075
	3.5–4	***	***	2089–2099	2076–2083
Late-century	4–4.5	***	***	***	2084–2092
High-end	4.5–5	***	***	***	2093–2099

5.2 months) for present-day conditions. In the near-future (1.5–2.0 °C), the median model year shows the route opening on DOY 169 (18 June) and closing on DOY 344 (10 December), giving an NP of 175 d – about 5.8 months and 18 d longer than present day. In the 4.5–5.0 °C anomaly range, the median model year shows opening on DOY 105 (15 April) and closing on DOY 409 (13 February of the following year), yielding 304 d (about 10.1 months) – around 129 d longer than the near-future and 147 d longer than present-day.

Under the ice-free definition, the present-day Chesterfield Inlet route (1.0–1.5 °C) typically opens on DOY 185 (3 July) and closes on DOY 324 (20 November) in the median model year, for a duration of 139 d (almost 4.6 months; Fig. 8). This is only a few days longer than the median year in the 2010s (according to OSISAF; Fig. 5). For near-future projections (1.5–2.0 °C), the Chesterfield Inlet route typically opens on DOY 176 (25 June) and closes on DOY 330 (26 November), yielding an NP of 154 d (approximately 5 months), about 15 d longer. On the extreme end, in the 4.5–5.0 °C anomaly bin, which is only reached under SSP5-8.5 near the end of the century (2093–2099; Table 1), the median model year opens on DOY 130 (10 May) and closes on DOY 376 (11 January of the following year), for a duration of 246 d (roughly 8.2 months), about 92 d longer than expected for the near-future (1.5–2.0 °C) and 107 d longer than the present-day anomaly bin (1.0–1.5 °C).

Under the low-risk definition, present-day results (1.0–1.5 °C) indicate that, in a typical year, the Chesterfield Inlet route opens on DOY 169 (18 June) and closes on DOY 326 (22 November), resulting in 157 d (roughly 5.2 months). In the near-future (1.5–2.0 °C), the route is projected to open on DOY 160 (9 June) and close on DOY 333 (29 November), giving an NP of 173 d – about 5.8 months, or 16 d longer than present-day conditions. On the extreme end (4.5–5.0 °C), the median model year opens on DOY 107 (17 April) and closes on DOY 391 (26 January of the following year), yielding 284 d (about 9.5 months) – around 111 d longer than the near-future and 127 d longer than present-day.

Table 2 summarizes how the median NP varies with increasing GSAT anomalies for the ice-free and low-risk definitions along the Labrador Sea and Chesterfield Inlet routes. Overall, the rate of lengthening NP with continued warming varies from 42 d °C^{-1} for the low-risk definition and Labrador Sea route to 31 d °C^{-1} for the ice-free definition and Chesterfield Inlet route. The sensitivity increases above a GSAT anomaly of 3.5 °C, with average rates of approximately 27–33 d °C^{-1} below 3.5 °C compared with approximately 35–55 d °C^{-1} above 3.5 °C, depending on route and definition. See Supplement Fig. S10 for the Arviat, Whale Cove, and Rankin Inlet routes.

3.4 Delta-Shift vs. Weighted Average

To evaluate the effectiveness of different bias correction strategies, we compared the results from the previous section with those obtained using a weighted average approach over the 1979–2024 period. Under the ice-free definition, the weighted average approach only leads to notable bias reduction in one of the two routes. For the Churchill-Labrador Sea route, OSISAF yields 111.0 d compared with a multi-model mean of 144.0 d (−33.0 d bias). The weighted average (127.1 d) reduces the bias to −16.1 d, representing a 51 % improvement. Using PIOMAS (119.1 d), the bias decreases from −24.9 to −7.9 d, a 68 % improvement. For the Churchill-Chesterfield Inlet route under the ice-free definition, OSISAF indicates 123.1 d compared with a multi-model mean of 158.4 d, yielding a bias of −35.3 d (already shown in Fig. 7). The weighted average gives 157.3 d, barely changing the bias, which is reduced only to −34.2 d (3 % improvement). A similar result is found if using PIOMAS (123.3 d) as the reference, where the bias decreases from −35.1 to −34.0 d (3 % improvement).

For the low-risk definition, in the Churchill-Labrador Sea route, PIOMAS gives 143 d compared with a multi-model

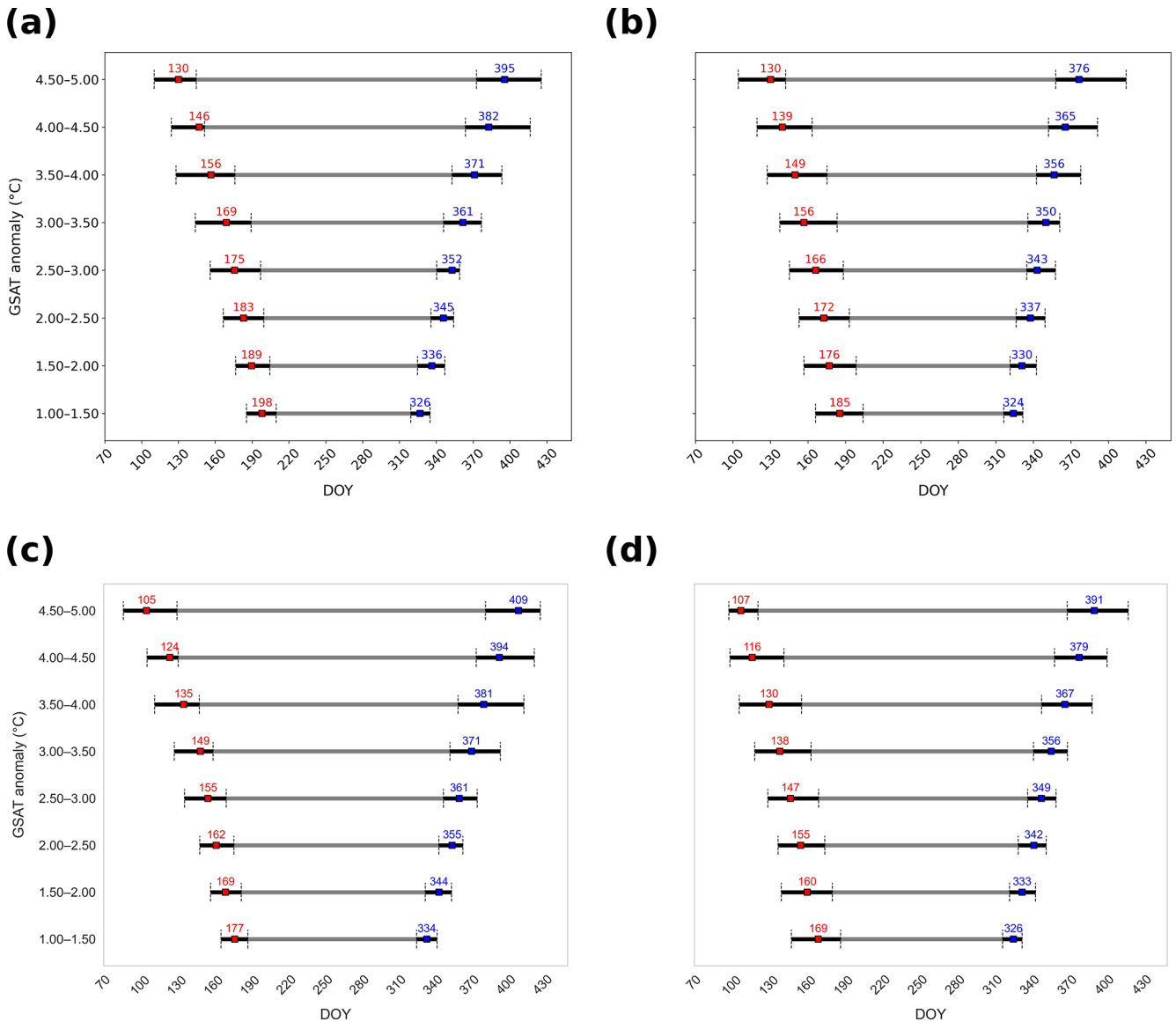


Figure 8. Projected opening and closing days (day of year, DOY) across global surface air temperature (GSAT) anomaly bins, estimated using the delta-shift bias correction method under SSP5-8.5. GSAT anomalies are relative to the 1850–1900 pre-industrial baseline. Results are shown for routes from the Port of Churchill to: **(a)** Labrador Sea (ice-free definition), **(b)** Chesterfield Inlet (ice-free definition), **(c)** Labrador Sea (Type E low-risk definition), and **(d)** Chesterfield Inlet (Type E low-risk definition). Red and blue markers represent the median opening day and closing day, respectively, with the interval between them indicating the median navigation period. Error bars denote the 10th–90th percentile range, and the grey bar highlights the period when the route is reliably navigable, except in extreme years.

mean of 157.3 d (bias: −14.3 d). After applying the weighted average (142.4 d), the bias is +0.6 d. This represents a 95.8 % improvement of the bias magnitude. In contrast, for the Churchill-Chesterfield Inlet route PIOMAS yields 146.5 d relative to a multi-model mean of 172.8 d (bias: −26.3 d). The weighted average correction (165.4 d) reduces the bias to −18.9 d, corresponding to a 28.1 % improvement.

Analysis of the projected NP under two bias correction approaches – delta-shift and weighted average – reveals substantial discrepancies across both routes and NP criteria (Fig. 9). For the Churchill-Labrador Sea route under the ice-free definition, the divergence is 17.37 d (11.7 %) in 2038, increasing to 32.85 d (12.4 %) by 2096 under SSP5-8.5. Conversely, under the low-risk definition, the difference in 2038 is minimal at 1.57 d (0.9 %), indicating close agreement between correction techniques. However, by 2096, under SSP5-8.5, the gap reaches 25.87 d (8.6 %). For the Churchill-Chesterfield Inlet route under the ice-free criterion, in 2038 the estimated NP differs by 35.25 d (23.0 %) between the two correction methods. This difference coincides with a

Table 2. Median navigable period (in days) for type E vessel under different global surface air temperature (GSAT) anomaly levels and SSP5-8.5 across the ice-free and low-risk conditions for the Labrador Sea and Chesterfield Inlet routes.

GSAT anomaly (°C)	Ice-free		Low-risk	
	Labrador Sea	Chesterfield Inlet	Labrador Sea	Chesterfield Inlet
1.00–1.50	128	139	157	157
1.50–2.00	147	154	175	173
2.00–2.50	162	165	193	187
2.50–3.00	177	177	206	202
3.00–3.50	192	194	222	218
3.50–4.00	215	207	246	237
4.00–4.50	236	226	270	263
4.50–5.00	265	246	304	284

GSAT anomaly of approximately 1.75 °C, consistent across all SSPs. By 2096 under SSP5-8.5, the divergence remains high at 26.45 d (10.2 %). Under the low-risk criterion for the same route, the projected difference is smaller but still significant: 27.37 d (15.7 %) in 2038, expanding to 30.06 d (10.6 %) by 2096 under SSP5-8.5.

Table 3 summarizes the projected navigable period (in days) over time under SSP5-8.5 for the ice-free and low-risk conditions along the Labrador Sea and Chesterfield Inlet routes using two bias correction methods. Collectively, these results show that both correction methods broadly capture the long-term increase in NP, although their projected values diverge substantially in some years, particularly in several late-century projections and for the ice-free definition. The discrepancies range from approximately 2 to 38 d (about 1 %–24 %, depending on method, route, and year), highlighting the sensitivity of NP projections to the choice of bias correction method. See Supplement Fig. S11 for the Arviat, Whale Cove, and Rankin Inlet routes.

3.5 Navigable Period for Different Vessel Types

Figure 10 examines how different vessel types affect the NP under historical period (1979–2013; panel a) and future warming levels (panel b) for the Labrador Sea route using the low-risk definition. In panel (a), the CMIP6 multi-model mean NP increases from 158 d for type E vessels to 225 d for Type IAA vessel, compared with the corresponding PIOMAS means of 140 and 191 d, respectively. The more ice-capable polar classes exhibit substantially longer navigable periods, with PC6 and PC5 reaching 258 and 351 d, respectively, compared with the corresponding PIOMAS means of 218 and 338 d. These results demonstrate that vessel ice capability is an important determinant of historical route accessibility and that the type E results represent a conservative lower bound on navigability rather than conditions representative of all vessel types.

In panel (b), the NP under the delta-shift bias-corrected CMIP6 multi-model mean for SSP5-8.5 generally increases with GSAT anomaly across all vessel types, although the magnitude of the response varies substantially by vessel type. The least ice-capable type E vessels show a pronounced increase in NP, from approximately 160 d at 1.0–1.5 °C warming to more than 300 d at 4.5–5.0 °C, indicating a transition toward near year-round accessibility under high-end warming. Intermediate vessel classes (IA, IAA, IB, and IC) also exhibit progressively longer NPs, while the more ice-capable PC classes maintain substantially longer navigation windows throughout the warming level, with PC5 remaining close to year-round accessibility. Vessel types with greater ice capability than PC5 (PC4 to PC1) reach year-round accessibility and are therefore not shown here. Nevertheless, type E vessels do not achieve continuous navigability under the high-end SSP5-8.5 scenario, indicating that year-round shipping would still require vessels with greater ice capability throughout the 21st century.

4 Discussion

Our results demonstrate that the choice of navigability criteria strongly influences the estimated length of the NP for open-water vessels in Hudson Bay and surrounding regions. The ice-free definition yields stricter thresholds, resulting in relatively short and constrained navigable windows. By contrast, the low-risk definition is more permissive, projecting NPs exceeding 10 months with 4.5–5.0 °C warming. This definition allows travel with various combinations of thickness and concentration, with 15 cm as the thickness limit for 100 % ice-coverage to be considered "low-risk" for type E (non-ice-strengthened or minimally ice-strengthened vessels) vessels. The deployment of higher-class vessels, such as those built to polar standards, would considerably extend the NP since these vessels can navigate through thicker ice without significant difficulty. Even with extreme warming scenarios and the most permissive criteria, ice-strengthened vessels would still be necessary for 12-month shipping along these routes.

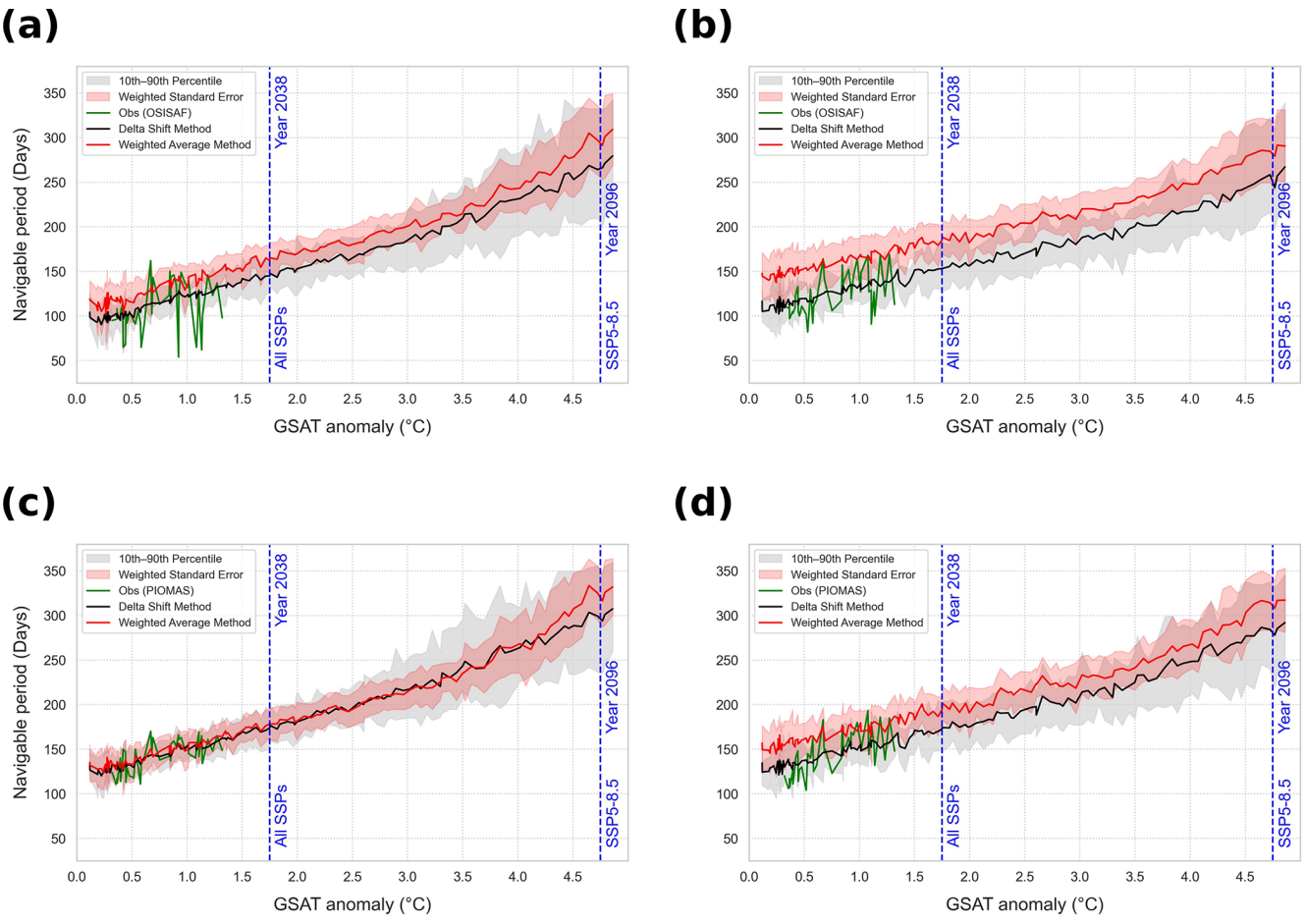


Figure 9. Projected navigable period (in days) as a function of global surface air temperature (GSAT) anomaly relative to the 1850–1900 baseline, under SSP5-8.5, for routes from the Port of Churchill to: **(a)** Labrador Sea (ice-free definition), **(b)** Chesterfield Inlet (ice-free definition), **(c)** Labrador Sea (Type E low-risk definition), **(d)** Chesterfield Inlet (Type E low-risk definition). Dashed blue vertical lines indicate the GSAT anomaly and SSP(s) for the two reference years discussed in the text.

Table 3. Projected navigable period (in days) over time for type E vessel under SSP5-8.5 across the ice-free and low-risk conditions for the Labrador Sea and Chesterfield Inlet routes using two bias correction methods.

Year	Delta shift				Weighted Average			
	Ice-free		Low-risk		Ice-free		Low-risk	
	Labrador Sea	Chesterfield Inlet	Labrador Sea	Chesterfield Inlet	Labrador Sea	Chesterfield Inlet	Labrador Sea	Chesterfield Inlet
2020	123	140	151	159	152	173	161	181
2030	138	147	168	167	153	182	170	190
2040	143	156	173	174	164	185	178	195
2050	164	171	194	192	177	200	192	212
2060	178	181	209	203	194	212	207	222
2070	196	193	228	219	206	218	219	229
2080	221	211	257	242	234	240	250	256
2090	239	230	281	267	268	268	294	290
2099	279	267	307	292	309	291	332	317

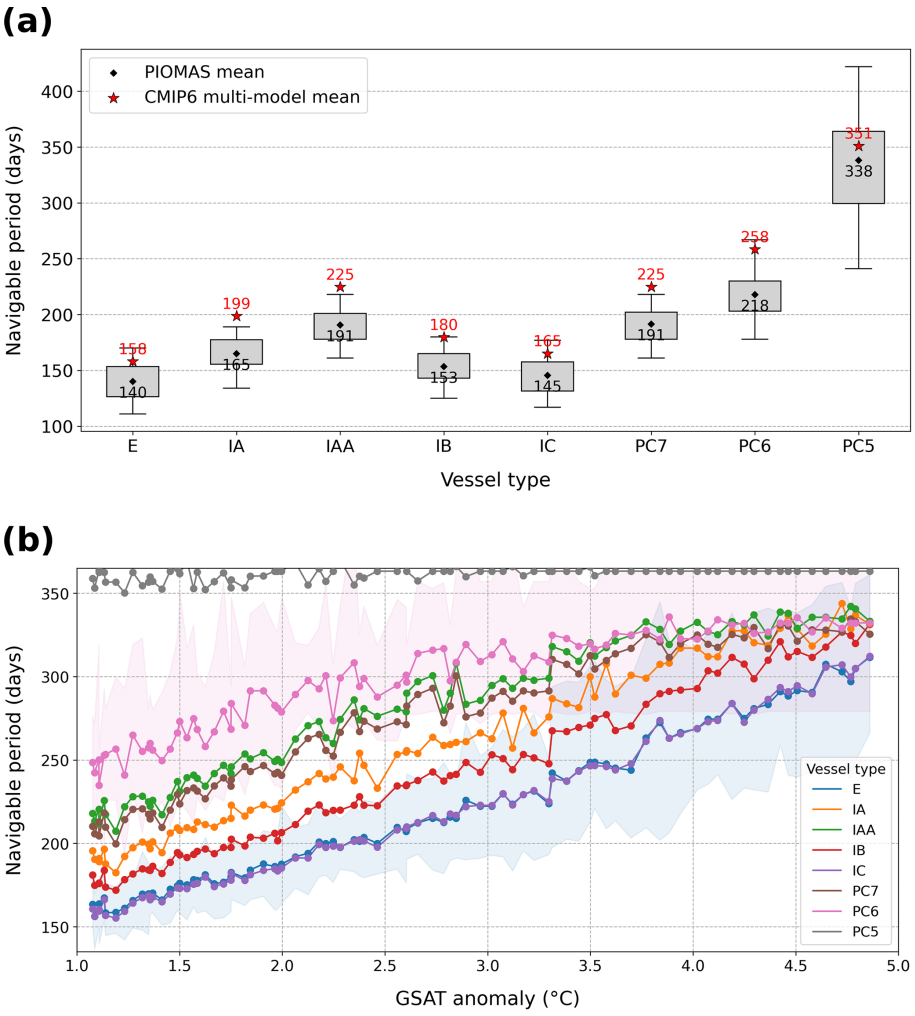


Figure 10. Navigable period (in days) for different vessel types in the Labrador Sea using low-risk definition: **(a)** Historical navigable period during 1979–2013 for the CMIP6 multi-model mean and PIOMAS mean, **(b)** Projected navigable period under SSP5-8.5 for the delta-shift bias-corrected CMIP6 multi-model mean. The CMIP6 10th–90th percentile range is shown as a shaded area for type E and PC6 vessels for illustration.

The bias correction framework applied here is central to improving the credibility of NP estimates. The delta-shift correction aligns closely with historical observations (by definition); however, the weighted average correction is valuable in preventing an overfit to the historical record. The delta-shift method implicitly assumes that historical conditions capture the full range of internal variability, but this assumption may not hold for long-term climate change projections. In contrast, the weighted average approach retains part of that variability, acknowledging that observations are not a perfect analogue for future conditions. This distinction highlights that both methods have value – delta-shift for fidelity to the observed record, and weighted average for preserving variability that may better capture future uncertainty. The weighted average method also yields smaller uncertainty in the future projections, so with the low-risk criterion, for which the weighted average also eliminates a large fraction of model-observation discrepancy, the weighted average result may be especially valuable (Fig. 9). However, for the ice-free criterion, especially when applied to the Chesterfield Inlet route, the lingering historical bias is so great in the weighted average that any projections with the weighted average should be considered with skepticism; the delta-shift method is preferred. With respect to long-term trends, the underestimation of the observed long-term trend by the multi-model mean for the Churchill-Chesterfield Inlet route under the low-risk definition suggests comparatively lower confidence in the projected magnitude of change, as opposed to the ice-free definition or the Labrador Sea route.

Accounting for uncertainty is critical when translating model output into decision-relevant information. Our use of the OD_{90}–CD_{10} framework provides a rigorous means of bracketing navigable periods into high-confidence, pessimistic, and optimistic estimates. For instance (see Fig. 8),

under the low-risk method, the Labrador Sea route exhibits a present-day NP of 157 d, representing the most likely navigability scenario. The pessimistic bound (138 d) reflects years when ice persists longer, while the optimistic bound (177 d) captures conditions under which the NP could be extended. We focused on the median outcomes here, but stakeholders such as shipping companies and insurers may prefer to consider the more pessimistic and optimistic outcomes and plan for a range of possible season lengths.

Despite differences in study area and methodology, our results can be placed in the context of other work in the literature. For example, Andrews et al. (2017), applying a 15 % SIC threshold, reported a median open-water season of 153 d in Hudson Bay for 2010–2014 – about 19 d longer than the period for which we are able to find continuous ice-free paths along the Churchill-Labrador Sea or Churchill-Chesterfield Inlet routes (Fig. 5). This discrepancy emphasizes the importance of identifying a continuous path rather than a spatial average for assessing route navigability. For future projections, Mudryk et al. (2021) provides the only comparable study, but our methods differ in several ways: (a) we calculate the RIO for individual grid cells with Eq. (1) and floe thickness, whereas they use effective thickness ($SIT_{eff} = SIT \times SIC$) and then RIO = RV ($SIT_{eff}$); (b) we identify the presence of any continuous route of navigable cells within a zone instead of using an area-weighted average RIO within that zone; (c) we use a multi-model ensemble from CMIP6 whereas they use a single-model ensemble from CESM1 and (d) we apply a bias correction to projections.

To assess the sensitivity of the NP to some of those methodological differences, we present NP estimates derived using different methodologies for the Churchill-Labrador Sea route (Table 4). We use method low-risk A (the method for the above results) as the baseline. For the historical period (1979–2013), using Eq. (2) but still using a continuous path-finding approach (method low-risk B) leads to a substantially shorter average NP than low-risk A (47 d shorter in PIOMAS and 55 d shorter in CMIP6). In fact, this NP is shorter than if using SIC < 15 % as the criterion for "navigable" (NP = 114 for the ice-free method).

The substantial difference noted above can be attributed to the fact that, in both PIOMAS and CMIP6, it is possible to have SIT exceed 1 m even when SIC < 15 %. For example, in 2013, method low-risk B yields a closing day of 309 (November 5), while the ice-free method yields a closing day of 322 (November 18) since SIC does not increase beyond 15 % until then (Supplement Fig. S12). The earlier closure for low-risk method B occurs because sea ice of low concentration (< 15 %) but thicker than 50 cm stretches across Hudson Strait. Using low-risk method A (Eq. 1), the route does not close until day 330 (November 26; Supplement Fig. S13), when sea ice in the 15–50 cm thickness range and a concentration of about 70 % blocks the route right at the Port of Churchill.

Method low-risk D also produces a shorter average NP relative to method low-risk A, but not as short as method low-risk B (18 d shorter in PIOMAS and 21 d shorter in CMIP6). In contrast, calculating cell-specific RIOs using Eq. (1) but averaging those RIO values over the entire route (method low-risk C) instead of requiring a continuous path leads to a longer average NP than method low-risk A (26 d longer in PIOMAS and 32 d longer in CMIP6).

The relative ordering of the four methods from longest to shortest NP is the same in the CMIP6 multi-model mean as in PIOMAS, although the sensitivity to choice of method is generally larger in CMIP6. For the historical period, the range of NPs calculated for PIOMAS spans 73 d depending on choice of method while for CMIP6 the range spans 87 d. These differences mean that the estimates of CMIP6 ensemble mean bias depend on the choice of method with a range of estimated bias values from approximately 1–3 weeks. However, for the future, the projected changes in NP are much less sensitive to the choice of method, with the four different methods yielding projected increases in NP of 75–84 d at a global warming level of 3 °C.

While it is reassuring that different methodological decisions yield similar projected changes (within 4 d 0.5 $°C^{-1}$ of global warming), we are still left with the problem that the calculated values for the historical NP in our reference dataset (PIOMAS) vary by more than 10 weeks and affect the uncertainty in estimated bias by about 2 weeks. Because bias is strongly regionally dependent, shipping routes elsewhere may be more or less sensitive to the choice of method than what we find here for Hudson Bay. It is important to note that, while method A and D both yield more moderate values for the NP, this occurs due to compensation in the methodological choices. Method A employs a more permissive RIO equation but a less permissive way to determine full-route navigability, whereas method D employs a less permissive RIO equation and a more permissive way (and arguably less realistic way) to determine full-route navigability. Methods B and C, which apply the least and most permissive combinations, respectively, result in rather extreme values for the NPs.

Because of this sensitivity, future work should attempt to constrain which methods are more accurate. However, there is an additional dimension to consider: certain methodological choices might be better suited for certain datasets. For example, Cook et al. (2024) used Canadian Ice Service Charts for their examination of the Northwest Passage. The ice charts contain information on ice types, which can equate to a range of ice thicknesses. Therefore, Cook et al. (2024) used a modified version of POLARIS with four consolidated categories that always took the most conservative RV in the grouping (e.g., their maximum RV for a type E vessel is 1 instead of 3). This choice may not be as applicable to a gridded dataset with explicit SIT values like PIOMAS. Similarly, Method A may be particularly well-suited for work with PIOMAS and CMIP6 because of the presence of thick sea ice at

Table 4. Sensitivity of the navigable period (NP, in days) to methodological choices (described in the text) and bias correction for the Churchill–Labrador Sea route.

Method	Consideration		1979–2013					2064–2088, SSP3-7.0	
	RIO equation	Route	PIOMAS		CMIP6			CMIP6	
			NP average	Diff vs. low-risk A	NP average	Diff vs. low-risk A	Bias	NP Average/ Bias corrected	Diff vs. low-risk A/ Bias corrected
Low-risk A	SIC × RV + 3× (1− SIC)	Continuous path	140	0	157	0	−17	232/215	0/0
Low-risk B	SIC × RV	Continuous path	93	−47	102	−55	−9	185/176	−47/−39
Low-risk C	SIC × RV + 3× (1− SIC)	Area avg. RIO	166	26	189	32	−23	273/250	41/35
Low-risk D	SIC × RV	Area avg. RIO	122	−18	136	−21	−14	220/206	−12/−9

low concentrations in Hudson Strait in these datasets – something other datasets might lack. Therefore, a comprehensive comparison would require comparison of all methodological choices across multiple datasets. Ideally, that would be conducted across multiple study areas and also compare opening and closing dates to actual ship operations in ice-infested water, including when ships become stuck and when they experienced uninterrupted travel.

Finally, it is important to note that the ice-free and low-risk NPs estimated here do not necessarily correspond directly to the operational shipping season. Actual vessel operations are also influenced by regulatory requirements, vessel characteristics, insurance considerations, and other operational constraints, which may restrict navigation during periods that meet the sea ice criteria (Andrews et al., 2017). Although these extended NPs may create significant economic opportunities for the Port of Churchill and northern trade, they may also present ecological and cultural challenges. Increased vessel traffic can affect the Hudson Bay marine ecosystem by disrupting marine mammal behaviour (Hauser et al., 2018), disturbing and degrading benthic habitats (Vincent et al., 2023), and introducing invasive or harmful species (Goldsmit et al., 2021).

5 Conclusion

Throughout this paper, we have demonstrated that calculations of navigable period are highly sensitive to methodological assumptions. In particular, we explored the dependence on (1) three formulations of grid-cell-specific navigable conditions (SIC $< 15\,\%$, and two formulations of POLARIS RIOs) (2) two definitions for determining full route navigability (presence of a continuously navigable path and route-averaged RIO values) and (3) two bias-correction methods (delta-shift and weighted ensemble). All cases indicate substantial lengthening of the navigable season with historical and future warming, and aken together, these results indicate that the navigable period for the Churchill-Labrador route increases by 13–19 d for every 0.5 °C of global warming regardless of methodological choices. Requiring a continuous ice-free route suggests the slowest lengthening (13–14 d 0.5 $°C^{-1}$). Using the RIO variation with Eq. (1) and requiring a contiguous route of navigable cells yields 15–16 d 0.5 $°C^{-1}$. Other RIO-based methods yield stronger increases of 17–18 d 0.5 $°C^{-1}$. These increases are consistent up to 3.5 °C of global warming, after which increases may accelerate.

Although the spread in projected change is reasonably small, we have also demonstrated that the calculated values of the navigable periods are much more sensitive to the method and can vary by more than 10 weeks. Using explicit calculations, we confirmed previous work suggesting a strong need to bias-correct model sea ice simulations for navigability projections. We demonstrated that CMIP6 models overestimate the NP duration by 1–3 weeks, with approximately 2 weeks of uncertainty in that bias value due to the methodological choices explored. While it is not straightforward to obtain accurate and precise observed values for historical navigable periods, we suggest that future work should focus on constraining the methodological choices that lead to better agreement with such historical values. Finally, we note that even with the strongest warming scenario (SSP5-8.5), no method yields year-round navigability for open water vessels, which indicates that year-round shipping in Hudson Bay would require ice-strengthened vessels throughout the 21st century.

Data availability. The data from the Ocean and Sea Ice Satellite Application Facility (OSISAF) are available at https://osi-saf.eumetsat.int/products/sea-ice-products (last access: 7 August 2025). The data from the Pan-Arctic Ice-Ocean Modeling and Assimilation System (PIOMAS) are available at https://psc.

apl.uw.edu/research/projects/arctic-sea-ice-volume-anomaly/data/ (last access: 6 November 2025). The data from the Coupled Model Intercomparison Project Phase 6 (CMIP6) are available at https://esgf.github.io/nodes.html (last access: 12 August 2025).

Supplement. The supplement related to this article is available online at https://doi.org/10.5194/tc-20-6613-2026-supplement.

Author contributions. Conceptualization, methodology, programming, analysis, and visualization were performed by A.S. and A.C. The original draft was prepared by A.S. Review and editing were conducted by L.M. Funding acquisition, project administration, supervision, and review and editing were conducted by A.C. and F.W. All authors have read and agreed to the published version of the manuscript.

Competing interests. The contact author has declared that none of the authors has any competing interests.

Disclaimer. Publisher's note: Copernicus Publications remains neutral with regard to jurisdictional claims made in the text, published maps, institutional affiliations, or any other geographical representation in this paper. The authors bear the ultimate responsibility for providing appropriate place names. Views expressed in the text are those of the authors and do not necessarily reflect the views of the publisher.

Financial support. This research was funded through the support of PrairiesCan, the Arctic Gateway Group, and the Government of Manitoba.

Review statement. This paper was edited by J.-F. Lemieux and reviewed by Minghu Ding and one anonymous referee.

References

Andrews, J., Babb, D., McKernan, M., Horton, B., and Barber, D.: Climate change in the Hudson Bay Complex: Opportunities and vulnerabilities for the Port of Churchill's Marine Operations, Tech. rep., University of Manitoba, Centre for Earth Observation Science, https://hdl.handle.net/1993/31138 (last access: 10 October 2025), 2016.

Andrews, J., Babb, D., and Barber, D. G.: Climate change and sea ice: Shipping accessibility on the marine transportation corridor through Hudson Bay and Hudson Strait (1980–2014), Elem. Sci. Anth., 5, 15, https://doi.org/10.1525/elementa.130, 2017.

Babb, D., Kirillov, S., Galley, R., Straneo, F., Ehn, J., Howell, S., Brady, M., Ridenour, N., and Barber, D.: Sea ice dynamics in Hudson Strait and its impact on winter shipping operations, J. Geophys. Res.-Oceans, 126, e2021JC018024, https://doi.org//10.1029/2021JC018024, 2021.

Cocetta, F., Zampieri, L., Selivanova, J., and Iovino, D.: Assessing the representation of Arctic sea ice and the marginal ice zone in ocean–sea ice reanalyses, The Cryosphere, 18, 4687–4702, https://doi.org/10.5194/tc-18-4687-2024, 2024.

Cook, A., Dawson, J., Holloway, J., Milton, M., Tagalik, S., Baker, K., Muckpah, J., Elverum, S., Boyse, E., Clark, M. S., Manno, C., Peck, V., and Risch, D.: Implications of changing shipping patterns near communities across Arctic Canada, Reg. Environ. Change, https://doi.org/10.1007/s10113-026-02599-7, 2026.

Cook, A. J., Dawson, J., Howell, S. E., Holloway, J. E., and Brady, M.: Sea ice choke points reduce the length of the shipping season in the Northwest Passage, Communications Earth & Environment, 5, 362, https://doi.org/10.1007/s10113-026-02599-7, 2024.

Copland, L., Dawson, J., Tivy, A., Delaney, F., and Cook, A.: Changes in shipping navigability in the Canadian Arctic between 1972 and 2016, Facets, 6, 1069–1087, https://doi.org/10.1139/facets-2020-0096, 2021.

Crawford, A., Stroeve, J., Smith, A., and Jahn, A.: Arctic open-water periods are projected to lengthen dramatically by 2100, Communications Earth & Environment, 2, 109, https://doi.org/10.1038/s43247-021-00183-x, 2021.

Crawford, A. D., Rosenblum, E., Lukovich, J. V., and Stroeve, J. C.: Sources of seasonal sea-ice bias for CMIP6 models in the Hudson Bay Complex, Ann. Glaciol., 64, 236–253, https://doi.org/10.1017/aog.2023.42, 2023.

EUMETSAT: Sea Ice Products, https://osi-saf.eumetsat.int/products/sea-ice-products (last access: 7 August 2025), 2025.

Eyring, V., Bony, S., Meehl, G. A., Senior, C. A., Stevens, B., Stouffer, R. J., and Taylor, K. E.: Overview of the Coupled Model Intercomparison Project Phase 6 (CMIP6) experimental design and organization, Geosci. Model Dev., 9, 1937–1958, https://doi.org/10.5194/gmd-9-1937-2016, 2016.

Ferguson, S. H., Young, B. G., Yurkowski, D. J., Anderson, R., Willing, C., and Nielsen, O.: Demographic, ecological, and physiological responses of ringed seals to an abrupt decline in sea ice availability, PeerJ, 5, e2957, https://doi.org/10.7717/peerj.2957, 2017.

Goldsmit, J., McKindsey, C. W., Stewart, D. B., and Howland, K. L.: Screening for High-Risk Marine Invaders in the Hudson Bay Region, Canadian Arctic, Frontiers in Ecology and Evolution, 9, https://doi.org/10.3389/fevo.2021.627497, 2021.

Hauser, D. D. W., Laidre, K. L., and Stern, H. L.: Vulnerability of Arctic marine mammals to vessel traffic in the increasingly ice-free Northwest Passage and Northern Sea Route, P. Natl. Acad. Sci. USA, 115, 7617–7622, https://doi.org/10.1073/pnas.1803543115, 2018.

Hochheim, K. P. and Barber, D. G.: An update on the ice climatology of the Hudson Bay system, Arct. Antarct. Alp. Res., 46, 66–83, https://doi.org/10.1657/1938-4246-46.1.66, 2014.

IMO Maritime Safety Committee: Guidance on Methodologies for Assessing Operational Capabilities and Limitations in Ice, Tech. Rep. MSC.1/Circ.1519, International Maritime Organization, London, UK, 2016.

IPCC: Summary for Policymakers, in: Climate Change 2021: The Physical Science Basis. Contribution of Working Group I to the Sixth Assessment Report of the Intergovernmental Panel on Climate Change, edited by Masson-Delmotte, V., Zhai, P., Pirani, A., Connors, S. L., Péan, C., Berger, S., Caud, N., Chen,

Y., Goldfarb, L., Gomis, M. I., Huang, M., Leitzell, K., Lonnoy, E., Matthews, J. B. R., Maycock, T. K., Waterfield, T., Yelekçi, O., Yu, R., and Zhou, B., 3–32, Cambridge University Press, Cambridge, United Kingdom and New York, NY, USA, https://doi.org/10.1017/9781009157896.001, 2021.

Knutti, R., Sedláček, J., Sanderson, B. M., Lorenz, R., Fischer, E. M., and Eyring, V.: A climate model projection weighting scheme accounting for performance and interdependence, Geophys. Res. Lett., 44, 1909–1918, https://doi.org/10.1002/2016GL072012, 2017.

Laidler, G. J. and Gough, W. A.: Climate variability and climatic change: potential implications for Hudson Bay coastal communities, Polar Geography, 27, 38–58, https://doi.org/10.1080/789610221, 2003.

Lasserre, F.: Canadian Arctic Marine Transportation Issues, Opportunities and Challenges, SPP Research Paper 15, The School of Public Policy, University of Calgary, Calgary, Canada, https://doi.org/10.11575/sppp.v15i1.72626, 2022.

Lavergne, T. and Down, E.: A climate data record of year-round global sea-ice drift from the EUMETSAT Ocean and Sea Ice Satellite Application Facility (OSI SAF), Earth Syst. Sci. Data, 15, 5807–5834, https://doi.org/10.5194/essd-15-5807-2023, 2023.

Lavergne, T., Sørensen, A. M., Kern, S., Tonboe, R., Notz, D., Aaboe, S., Bell, L., Dybkjær, G., Eastwood, S., Gabarro, C., Heygster, G., Killie, M. A., Brandt Kreiner, M., Lavelle, J., Saldo, R., Sandven, S., and Pedersen, L. T.: Version 2 of the EUMETSAT OSI SAF and ESA CCI sea-ice concentration climate data records, The Cryosphere, 13, 49–78, https://doi.org/10.5194/tc-13-49-2019, 2019.

MarineTraffic: Live Ship Tracking and Maritime Analytics, https://www.marinetraffic.com (last access: 1 January 2025), 2025.

Maslowski, W., Clement Kinney, J., Higgins, M., and Roberts, A.: The future of Arctic sea ice, Annu. Rev. Earth Pl. Sc., 40, 625–654, https://doi.org/10.1146/annurev-earth-042711-105345, 2012.

Meier, W. N., Peng, G., Scott, D. J., and Savoie, M. H.: Verification of a new NOAA/NSIDC passive microwave sea-ice concentration climate record, Polar Res., 33, 21004, https://doi.org/10.3402/polar.v33.21004, 2014.

Melia, N., Haines, K., and Hawkins, E.: Improved Arctic sea ice thickness projections using bias-corrected CMIP5 simulations, The Cryosphere, 9, 2237–2251, https://doi.org/10.5194/tc-9-2237-2015, 2015.

Mudryk, L. R., Dawson, J., Howell, S. E., Derksen, C., Zagon, T. A., and Brady, M.: Impact of 1, 2 and 4 °C of global warming on ship navigation in the Canadian Arctic, Nat. Clim. Change, 11, 673–679, https://doi.org/10.1038/s41558-021-01087-6, 2021.

Notz, D. and SIMIP Community: Arctic sea ice in CMIP6, Geophys. Res. Lett., 47, e2019GL086749, https://doi.org/10.1029/2019GL086749, 2020.

O'Neill, B. C., Tebaldi, C., van Vuuren, D. P., Eyring, V., Friedlingstein, P., Hurtt, G., Knutti, R., Kriegler, E., Lamarque, J.-F., Lowe, J., Meehl, G. A., Moss, R., Riahi, K., and Sanderson, B. M.: The Scenario Model Intercomparison Project (ScenarioMIP) for CMIP6, Geosci. Model Dev., 9, 3461–3482, https://doi.org/10.5194/gmd-9-3461-2016, 2016.

Pizzolato, L., Howell, S. E., Dawson, J., Laliberté, F., and Copland, L.: The influence of declining sea ice on shipping activity in the Canadian Arctic, Geophys. Res. Lett., 43, 12–146, https://doi.org/10.1002/2016GL071489, 2016.

Polar Science Center, University of Washington: PIOMAS Arctic Sea Ice Volume and Thickness Data (version 2.1), https://psc.apl.uw.edu/research/projects/arctic-sea-ice-volume-anomaly/data/ (last access: 6 November 2025), 2025.

Roach, L. A. and Meier, W. N.: Sea ice in 2023, Nature Reviews Earth & Environment, 5, 235–237, https://doi.org/10.1038/s43017-024-00542-0, 2024.

Shibata, H., Izumiyama, K., Tateyama, K., Enomoto, H., and Takahashi, S.: Sea-ice coverage variability on the Northern Sea Routes, 1980–2011, Ann. Glaciol., 54, 139–148, https://doi.org/10.3189/2013aog62a123, 2013.

Smith, L. C. and Stephenson, S. R.: New Trans-Arctic shipping routes navigable by midcentury, P. Natl. Acad. Sci. USA, 110, E1191–E1195, https://doi.org/10.1073/pnas.1214212110, 2013.

Solakivi, T., Kiiski, T., and Ojala, L.: The impact of ice class on the economics of wet and dry bulk shipping in the Arctic waters, Marit. Policy Manag., 45, 530–542, https://doi.org/10.1080/03088839.2018.1443226, 2018.

Soleymani, A. and Scott, K. A.: Arctic marginal ice zone interannual variability and change point detection using two definitions (1983–2022), Environ. Res. Lett., 18, 124002, https://doi.org/10.1088/1748-9326/ad0609, 2023.

Soriot, C., Vancoppenolle, M., Prigent, C., Jimenez, C., and Frappart, F.: Winter arctic sea ice volume decline: uncertainties reduced using passive microwave-based sea ice thickness, Sci. Rep., 14, 21000, https://doi.org/10.1038/s41598-024-70136-9, 2024.

Soriot, C., Stroeve, J., and Crawford, A.: Record early sea ice loss in southeastern Hudson Bay in Spring 2024, Geophys. Res. Lett., 52, e2024GL112584, https://doi.org/10.1029/2024GL112584, 2025.

Stroeve, J., Crawford, A., Ferguson, S., Stirling, I., Archer, L., York, G., Babb, D., and Mallett, R.: Ice-free period too long for Southern and Western Hudson Bay polar bear populations if global warming exceeds 1.6 to 2.6 °C, Communications Earth & Environment, 5, 296, https://doi.org/10.1038/s43247-024-01430-7, 2024.

Swart, N. C., Fyfe, J. C., Hawkins, E., Kay, J. E., and Jahn, A.: Influence of internal variability on Arctic sea-ice trends, Nat. Clim. Change, 5, 86–89, 2015.

The Earth System Grid Federation: ESGF Nodes, https://esgf.github.io/nodes.html (last access: 12 August 2025), 2025.

Tivy, A., Howell, S. E., Alt, B., McCourt, S., Chagnon, R., Crocker, G., Carrieres, T., and Yackel, J. J.: Trends and variability in summer sea ice cover in the Canadian Arctic based on the Canadian Ice Service Digital Archive, 1960–2008 and 1968–2008, J. Geophys. Res.-Oceans, 116, C03007, https://doi.org/10.1029/2009JC005855, 2011.

Vincent, W. F., Lovejoy, C., and Bartenstein, K.: Chapter 3 Shipping in Arctic Marine Ecosystems under Stress: Recognizing and Mitigating the Threats, Brill, Nijhoff, Leiden, The Netherlands, 37–57, https://doi.org/10.1163/9789004508576_004, 2023.

Wei, T., Yan, Q., Qi, W., Ding, M., and Wang, C.: Projections of Arctic sea ice conditions and shipping routes in the twenty-first century using CMIP6 forcing scenarios, Environ. Res. Lett., 15, 104079, https://doi.org/10.1088/1748-9326/abb2c8, 2020.

Zhang, J. and Rothrock, D. A.: Modeling global sea ice with a thickness and enthalpy distribution model in generalized curvilinear coordinates, Mon. Weather Rev., 131, 845–861, https://doi.org/10.1175/1520-0493(2003)131<0845:MGSIWA>2.0.CO;2, 2003.

Zhao, J., Shu, Q., Li, C., Wu, X., Song, Z., and Qiao, F.: The role of bias correction on subseasonal prediction of Arctic sea ice during summer 2018, Acta Oceanol. Sin., 39, 50–59, https://doi.org/10.1007/s13131-020-1578-0, 2020.